Electronic Supplementary Material (ESI) for Journal of Materials Chemistry C.
This journal is © The Royal Society of Chemistry 2023

SUPPORTING INFORMATION

Effect of Benzothiadiazole Spacer on Transport Properties and N-doping of Naphthalene-diimide-based Copolymers

Olivier Bardagot,[*a,b] *Yann Kervella,*[b] *Asma Aicha Medjahed,*[b,c] *Stéphanie Pouget,*[d] *Tamara Nunes Domschke,*[e] *Alexandre Carella,*[e,f] *Cyril Aumaitre,*[b] *Patrick Lévêque,*[g] *Renaud Demadrille.**[b]

a. Institute of Chemistry and Processes for Energy Environment and Health (ICPEES), CNRS, University of Strasbourg, UMR 7515, 25 rue de Becquerel, Strasbourg Cedex 02, 67087, France

b. Université Grenoble Alpes CEA CNRS IRIG-SyMMES Grenoble 38000, France

c. The European Synchrotron, Avenue des Martyrs 71, Grenoble 38000, France Université Grenoble Alpes

d. CEA, IRIG-MEM, Grenoble 38000, France

e. Université Grenoble Alpes CEA-LITEN Grenoble 38000, France

f. CEA, DES, ISEC, DMRC, Univ. Montpellier, Marcoule, 30 207, France

g. Laboratoire des Sciences de l'Ingénieur, de l'Informatique et de l'Imagerie (ICube Research Institute), Université de Strasbourg, CNRS, 23, Rue du Loess, Strasbourg Cedex 2 67037, France

*Corresponding authors email: olivier.bardagot@cnrs.fr, renaud.demadrille@cea.fr

TABLE OF CONTENTS

1. Polymer synthesis and characterization

1.1. Monomer synthesis

All chemicals were purchased from Merck KGaA-Sigma-Aldrich, Fluorochem, and Acros Organics and used as received.

Nuclear Magnetic Resonance (NMR) spectra were recorded using Bruker AC400 or AC500 spectrometers. Chemical shift, in ppm, and coupling constants, in Hertz, were determinate using MestReNova software (version 6.0.2-5475). The following abbreviation are used to describe the signals: s (singlet), d (doublet), t (triplet), q (quartet), m (multiplet), br (broad).

3-dodecyl-2,2'-bithiophene (1)

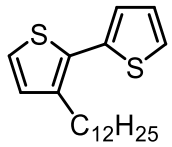

To a stirred solution of 3-dodecyl-2-iodothiophene (1.50 g, 3.94 mmol, 1.00 eq) and thiophen-2-ylboronic acid (0.65 g, 5.11 mmol, 1.30 eq) in a mixture of THF and deionized water (2:1 vol%, 60 mL), tripotassium phosphate (1.77 g, 8.35 mmol, 2.10 eq) is added. The reaction mixture is degassed prior to the addition of tetrakis(triphenylphosphine)palladium(0) (160 mg, 0.14 mmol, 0.35 eq) and stirred at 80°C for 4h40. The mixture is concentrated under reduced pressure and extracted with diethyl ether (3x20 mL). The organic layer is washed with deionized water (3x30 mL), and brine (20 mL), dried over Na_2SO_4, filtered and concentrated under reduced pressure. The resulting crude solution is purified by column chromatography (SiO_2, pentane 100 %) affording the pure compound as a colorless oil (756 mg, 2.26 mmol, 57 %).

Chemical formula: $C_{20}H_{30}S_2$

Molecular weight: 334.58 g mol^{-1}

^{1}H NMR ($CDCl_3$, 400 MHz, 298 K): δ (ppm) = 7.31 (dd, ^3J = 5.1 Hz, ^4J = 1.2 Hz, 1H), 7.18 (d, ^3J = 5.2 Hz, 1H), 7.12 (dd, ^3J = 3.6 Hz, ^4J = 1.2 Hz, 1H), 7.07 (dd, ^3J = 5.1 Hz, ^3J = 3.6 Hz, 1H), 6.95 (d, ^3J = 5.2 Hz, 1H), 2.74 (m, 2H), 1.67-1.57 (m, 2H), 1.39-1.21 (m, 18H), 0.90 (t, ^3J = 6.8 Hz, 3H).

^{13}C NMR ($CDCl_3$, 100 MHz, 298 K): δ (ppm) = 139.7, 136.2, 130.5, 129.9, 127.3, 126.0, 125.2, 123.7, 31.9, 30.7, 29.7, 29.6, 29.6, 29.5, 29.4, 29.3, 29.1, 22.7, 14.1.

All characterization data are in accordance with the literature.[1,2]

(3-dodecyl-[2,2'-bithiophene]-5,5'-diyl)bis(trimethylstannane) (2)

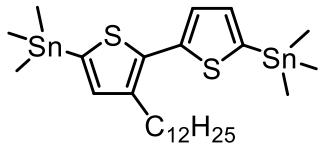

To a stirred solution of 3-dodecyl-2,2'-bithiophene **(1)** (840 mg, 2.50 mmol, 1.00 eq) in freshly distilled and freeze-pump-thaw degassed THF (20 mL), *n*-BuLi (2.5 M in hexanes, 2.1 mL, 5.25 mmol, 2.10 eq) is added dropwise at -78°C under argon. The addition induces a color change from pink to cyan. The reaction mixture is stirred at -78°C for 1 h prior to the addition of trimethyl tin chloride (1.0 M in THF, 5.3 mL, 5.24 mmol, 2.10 eq) in one portion. The mixture is stirred for further 30 min at -78°C and then allowed to warm up to room temperature. The reaction mixture is poured into 2.0 M aqueous NH_4Cl (100 mL) and extracted with diethyl ether (3x50 mL). The combined organic layer is washed with 2.0 M aqueous NH_4Cl (3x50 mL) and deionized water, dried over Na_2SO_4, filtered and dried under vacuum, affording the product as a green oil (1.41 g, 2.14 mmol, 85 %). A purity of 95 % was estimated by ^{1}H NMR.

Chemical formula: $C_{26}H_{46}S_2Sn_2$

Molecular weight: 660.19 g mol^{-1}

^{1}H NMR (Acetone-d6, 400 MHz, 298 K): δ (ppm) = 7.24 (d, ^{3}J = 3.4 Hz, 1H), 7.21 (d, ^{3}J = 3.4 Hz, 1H), 7.10 (s, 1H), 2.81-2.75 (m, 2H), 1.70-1.59 (m, 2H), 1.43-1.24 (m, 18H), 0.88 (t, ^{3}J = 7.0 Hz, 3H), 0.56-0.20 (m, 18H).

2-octyldodecyl 4-methylbenzenesulfonate (3)

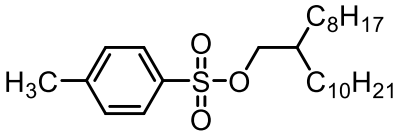

To a 0°C stirred solution of 2-octyldodecan-1-ol (4.00 mL, 3.35 g, 11,23 mmol, 1.00 eq) in $CHCl_3$ (15 mL) is added pyridine (1.33 g, 16.84 mmol, 1.50 eq), followed by the addition of p-toluenesulfonyl chloride (4.28 g, 22.45 mmol, 2.00 eq) in small portions. The reaction mixture is stirred at 0°C for 22 h. The reaction mixture is poured into 2.0 M aqueous HCl and

diluted with diethyl ether (60 mL). The organic layer is washed with 2.0 M aqueous HCl, 5 wt% $NaHCO_3$ and deionized water, dried over Na_2SO_4, filtered and concentrated under reduced pressure. The resulting crude product is purified by column chromatography (SiO_2, diethyl ether:petroleum ether – 2:98) affording the pure compound as a colorless oil (5.08 g, 11.23 mmol, quantitative).

Chemical formula: $C_{27}H_{48}O_3S$

Molecular weight: 452.74 g mol^{-1}

^{1}H NMR ($CDCl_3$, 400 MHz, 298 K): δ (ppm) = 7.78 (d, ^{3}J = 8.3 Hz, 2H), 7.34 (dd, ^{3}J = 8.6 Hz, ^{4}J = 0.6 Hz, 2H), 3.90 (d, ^{3}J = 5.3 Hz, 2H), 2.45 (s, 3H), 1.61-1.53 (m, 1H), 1.32-1.09 (m, 32H), 0.88 (t, ^{3}J = 7.0 Hz, 6H).

^{13}C NMR ($CDCl_3$, 100 MHz, 298 K): δ (ppm) = 144.5 (1C), 133.2 (1C), 129.7 (2C), 127.9 (2C), 72.9 (1C), 37.6 (1C), 31.9 (2C), 30.6 (2C), 29.8 (2C), 29.6 (2C), 29.5 (2C), 29.3 (2C), 26.5 (2C), 22.7 (2C), 21.6 (1C), 14.1 (2C).

All characterization data are in accordance with the literature.[3]

9-(azidomethyl)nonadecane (4)

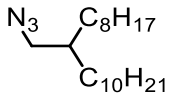

To a 50°C stirred solution of 2-octyldodecyl-4-methylbenzenesulfonate **(3)** (2.00 g, 4.42 mmol, 1.00 eq) in anhydrous DMF (18 mL) is added sodium azide (862 mg, 13.25 mmol, 3.00 eq) under argon. The mixture is stirred for 10 min at this temperature, then heated up to 90°C and stirred for further 16 h. The reaction mixture is allowed to cool down to room temperature and diluted with diethyl ether (70 mL). The organic layer is washed with deionized water and brine (3x30 mL), dried over Na_2SO_4, filtered and concentrated under reduced pressure, affording the crude product as a light yellow oil (1.14 g, 3.52 mmol, 80 %).

Chemical formula: $C_{20}H_{41}N_3$

Molecular weight: 323.57 g mol^{-1}

^{1}H NMR ($CDCl_3$, 400 MHz, 298 K): δ (ppm) = 3.22 (d, ^{3}J = 5.9 Hz, 2H), 1.54 (m, 1H), 1.32-1.26 (m, 32H), 0.88 (t, ^{3}J = 7.0 Hz, 6H).

All characterization data are in accordance with the literature.[4]

2-octyldodecan-1-amine (5)

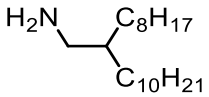

To a stirred solution of 9-(azidomethyl)nonadecane **(4)** (1.14 g, 3.52 mmol, 1.00 eq) in anhydrous THF (10 mL) is added triphenylphosphine (1.11 g, 4.23 mmol, 1.20 eq) under argon. The reaction mixture is stirred at 70°C for 17 h before addition of 2.5 mL of deionized water. The mixture is stirred for further hour at this temperature. The reaction mixture is allowed to cool down, concentrated under reduced pressure and diluted with diethyl ether (70 mL). The organic layer is washed with deionized water and brine, dried over Na_2SO_4, filtered and concentrated under reduced pressure. The resulting crude product is purified by column chromatography (SiO_2, petroleum ether:DCM - 2:8). Final purification is achieved by trituration in pentane (150 mL). The pentane solution is filtered and the filtrate is dried under vacuum, affording the pure compound as a colorless oil (1.04 g, 3.48 mmol, 99 %).

Chemical formula: $C_{20}H_{43}N$

Molecular weight: 297.57 g mol^{-1}

^{1}H NMR ($CDCl_3$, 400 MHz, 298 K): δ (ppm) = 2.62 (d, ^{3}J = 5.5 Hz, 2H), 2.03 (m, 1H), 1.45-1.22 (m, 32H), 0.88 (t, ^{3}J = 7.0 Hz, 6H).

All characterization data are in accordance with the literature.[5]

4,9-dibromoisochromeno[6,5,4-def]isochromene-1,3,6,8-tetraone (6)

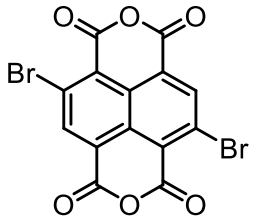

To a stirred solution of oleum (200 mL, 20-30 % SO_3) (CAUTION: TOXIC VAPOR), naphthalene dianhydride (10.00 g, 37.29 mmol, 1.00 eq) is added by portions. The suspension is stirred at 50°C for 30 min to reach complete solubilization prior to the careful addition of a catalytic amount of solid iodine (50 mg, 0,20 mmol, 0.05 eq). Then bromine (35.75 g, 11.5 mL, 223.73

mmol, 6.00 eq) solubilized in oleum (50 mL, 20-30 % SO_3) is added dropwise using a dropping funnel. The mixture at a total concentration of 0.15 M is stirred at 100°C for 40 h. The reaction mixture is allowed to cool down to room temperature and carefully poured over ice (CAUTION: EXOTHERMIC REACTION). The crude yellow precipitate is collected by filtration, washed with deionized water until neutral and dried under vacuum, affording crude brominated naphthalene dianhydride mixture as a light yellow precipitate used without further purification (15.88 g, 37.28 mmol, quantitative).

Chemical formula: $C_{14}H_2Br_2O_6$

Molecular weight: 425.97 g mol^{-1}

4,9-dibromo-2,7-dioctylbenzo[lmn][3,8]phenanthroline-1,3,6,8(2H,7H)-tetraone (7a)

This molecule was synthesized only to optimized the synthetic route of **(7)**.

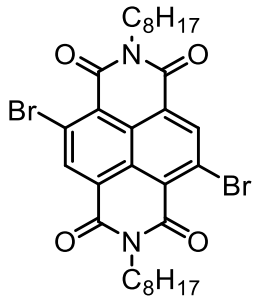

To a suspension of crude **(6)** (425 mg, 1.00 mmol, 1.00 eq) in conc. glacial AcOH (99 %, 5.0 mL, 0.2 M) in a 10 mL flask, octylamine (548 mg, 4.24 mmol, 4.25 eq) is added dropwise. The reaction mixture is sonicated at room temperature for 30 min. The reaction flask is then placed in a synthetic microwave with IR temperature feedback (Milestone). The stirring reaction mixture is evenly ramped to 110°C over 5 min (250W), and held to 110°C for 20 min (150W). The reaction is allowed to slowly cool down to room temperature over 30 min, resulting in the formation of a red-orange solid. The precipitate is collected by filtration, washed with glacial AcOH (3x2 mL), and dried under vacuum affording the pure dibromo compound as a pale yellow solid (158 mg, 0.24 mmol, 37 % over two steps).

Chemical formula: $C_{30}H_{36}Br_2N_2O_4$

Molecular weight: 648.44 g mol^{-1}

^{1}H NMR ($CDCl_3$, 400 MHz, 298 K): δ (ppm) = 9.00 (s, 2H), 4.19 (m, 4H), 1.74 (m, 4H), 1.45-1.20 (m, 20H), 0.90 (t, ^{3}J = 6.9 Hz, 6H).

All characterization data are in accordance with the literature.[6]

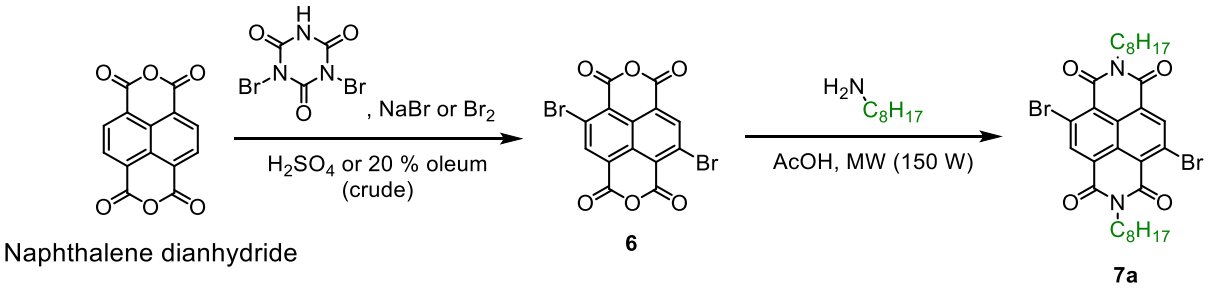

Bromination agent	Solvent	Concentration (mol L^{-1})	T (°C)	Time (h)	Total yield (%)
Dibromoisocyanuric acid	H_2SO_4	0.09	130	48	11
NaBr	H_2SO_4	0.1	150	16	0.5
NaBr	Oleum	0.1	150	16	14
NaBr	Oleum	0.1	150+110	3+69	8
Br_2	Oleum	0.37	100	44	5
Br_2	**Oleum**	**0.15**	**100**	**40**	**37**

Figure S1. Synthesis routes used for the bromination optimization of the naphthalene dianhydride. Summary of the conditions tested and total yield of (7a) over two steps.

4,9-dibromo-2,7-bis(2-octyldodecyl)benzo[lmn][3,8]phenanthroline-1,3,6,8(2H,7H)-tetraone (7)

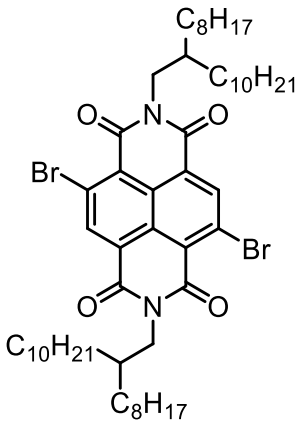

To a suspension of crude **(6)** (2.00 g, 4.70 mmol, 1.00 eq) in conc. glacial AcOH (99 %, 23.5 mL, 0.2 M) in a 50 mL flask, 2-octyldodecan-1-amine **(3)** (5.94 g, 19.95 mmol, 4.25 eq) is added dropwise. The reaction mixture is sonicated at room temperature for 30 min. The reaction flask is then placed in a synthetic microwave with IR temperature feedback (Milestone). The stirring reaction mixture is evenly ramped to 100°C over 5 min (250W), and held to 100°C for 1 h (150W). The reaction is allowed to slowly cool down to room temperature over 30 min. The mixture is concentrated under reduced pressure and extracted with DCM. The organic layer is washed with deionized water and brine, dried over Na_2SO_4, filtered and concentrated under reduced pressure. The resulting crude solution is purified by trituration in methanol (100 mL) at room temperature. The gold color solution is discarded and the dark red oil is further purified by column chromatography (SiO_2, *n*-hexane:DCM - 5:5). Final purification is achieved by recrystallization from *n*-hexane. The solid product is collected by filtration at 0°C and dried under vacuum, affording the pure compound as a pale yellow solid (1.52 g, 1.54 mmol, 33 % over two steps).

Chemical formula: $C_{54}H_{84}Br_2N_2O_4$

Molecular weight: 985.08 g mol^{-1}

^{1}H NMR ($CDCl_3$, 400 MHz, 298 K, d1 = 4sec): δ (ppm) = 9.00 (s, 2H), 4.15 (d, ^3J = 7.4 Hz, 4H), 1.99 (m, 2H), 1.47-1.11 (m, 64H), 0.93-0.80 (m, 12H).

^{13}C NMR ($CDCl_3$, 100 MHz, 298 K): δ (ppm) = 161.1, 139.1, 128.4, 127.7, 125.3, 124.1, 45.4, 36.5, 31.9, 31.6, 30.0, 29.6, 29.3, 26.3, 22.7, 14.1.

Negative-mode MALDI-TOF MS (337nm, calibrated TGT $[M-H]^-$ = 874.18 and 6Tyr $[M-H]^-$ = 995.38): m/z calcd. for $C_{54}H_{84}Br_2N_2O_4^{\bullet-}$: 984.48 (100.0 %); Found: 984.39.

ESI MS (calibrated TGT $[M-H]^-$ = 874.2): m/z calcd. for $C_{54}H_{84}Br_2N_2O_4^{\bullet-}$: 984.48 (100.0 %); Found: 984.4.

All characterization data are in accordance with the literature on the same compound with 2-decyltetradecane alkyl chains.[7]

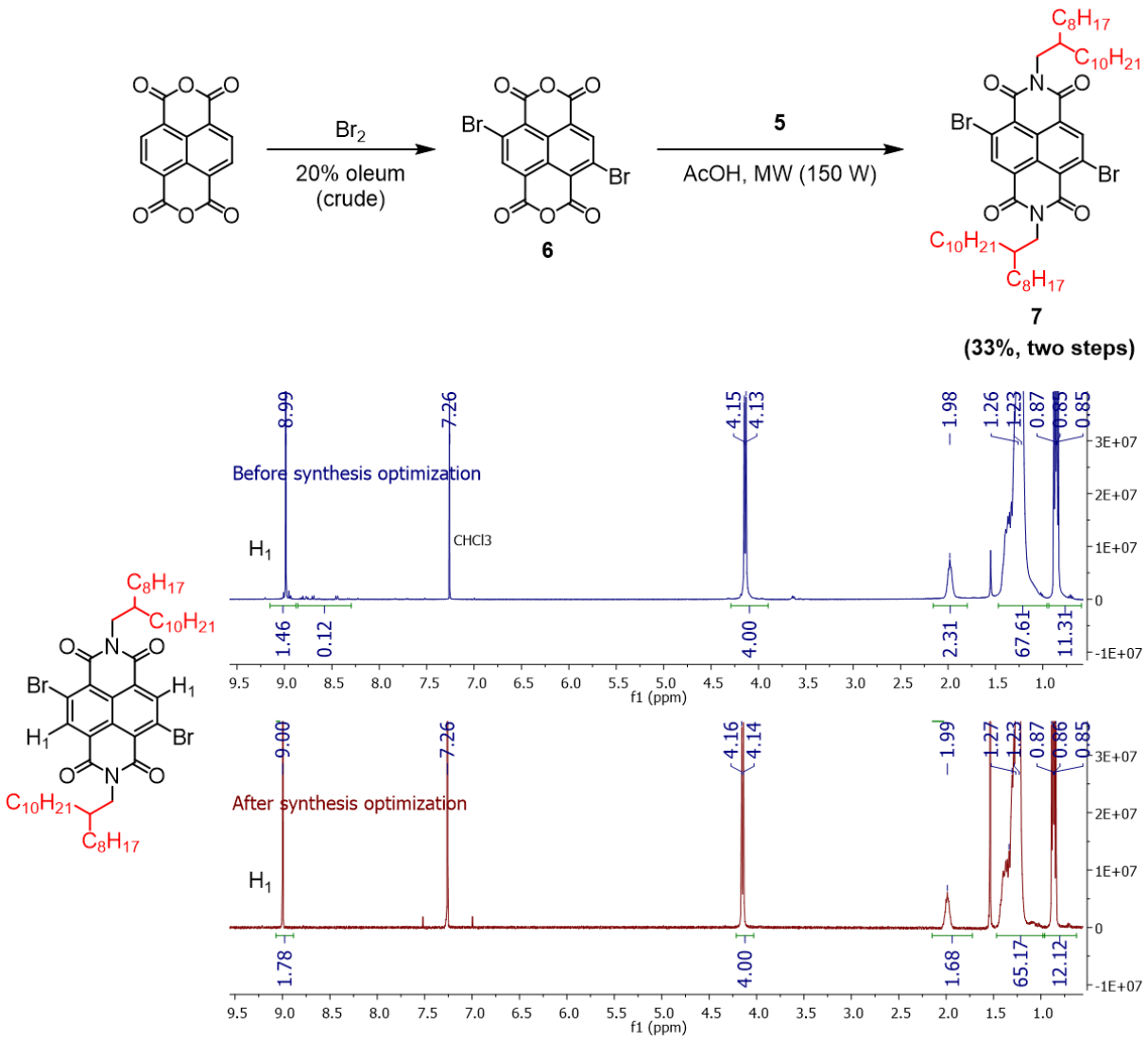

Figure S2. Synthesis route of NDI-BR_2 monomer **(7)**, and corresponding ^{1}H NMR spectra in $CDCl_3$ before and after optimization of the bromination reaction.

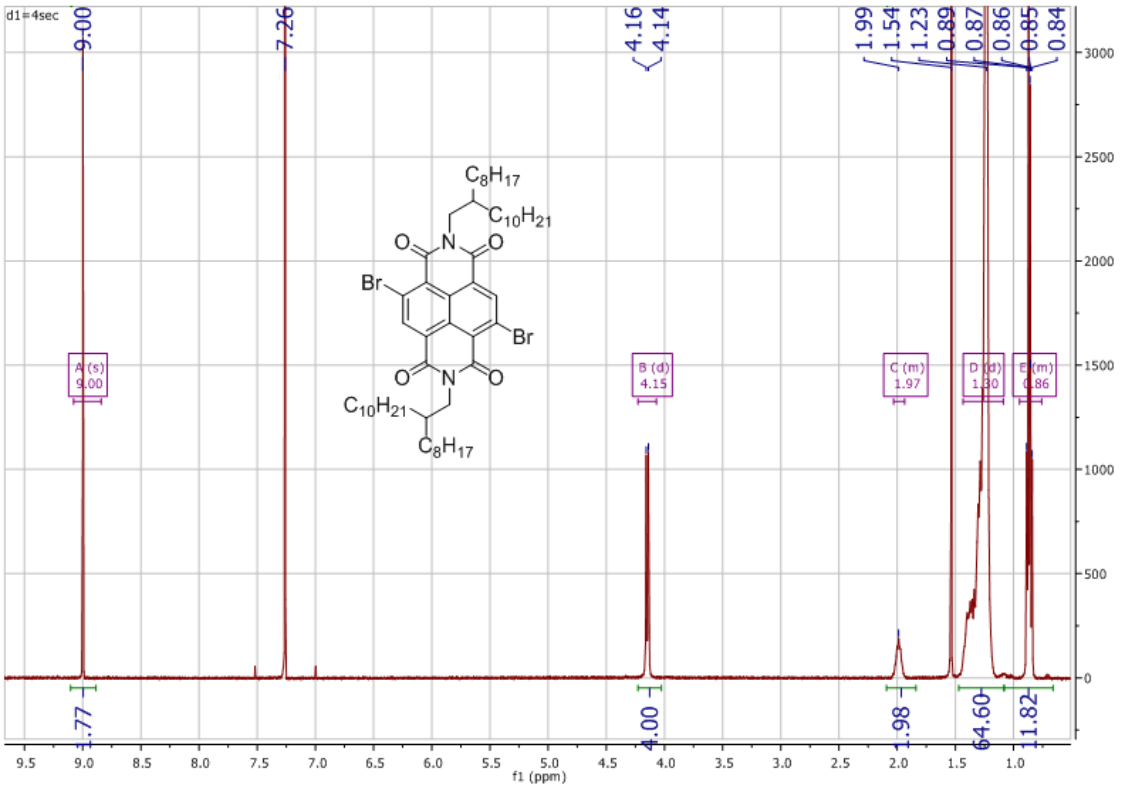

Figure S3. ^{1}H NMR spectrum of compound **(7)** in $CDCl_3$.

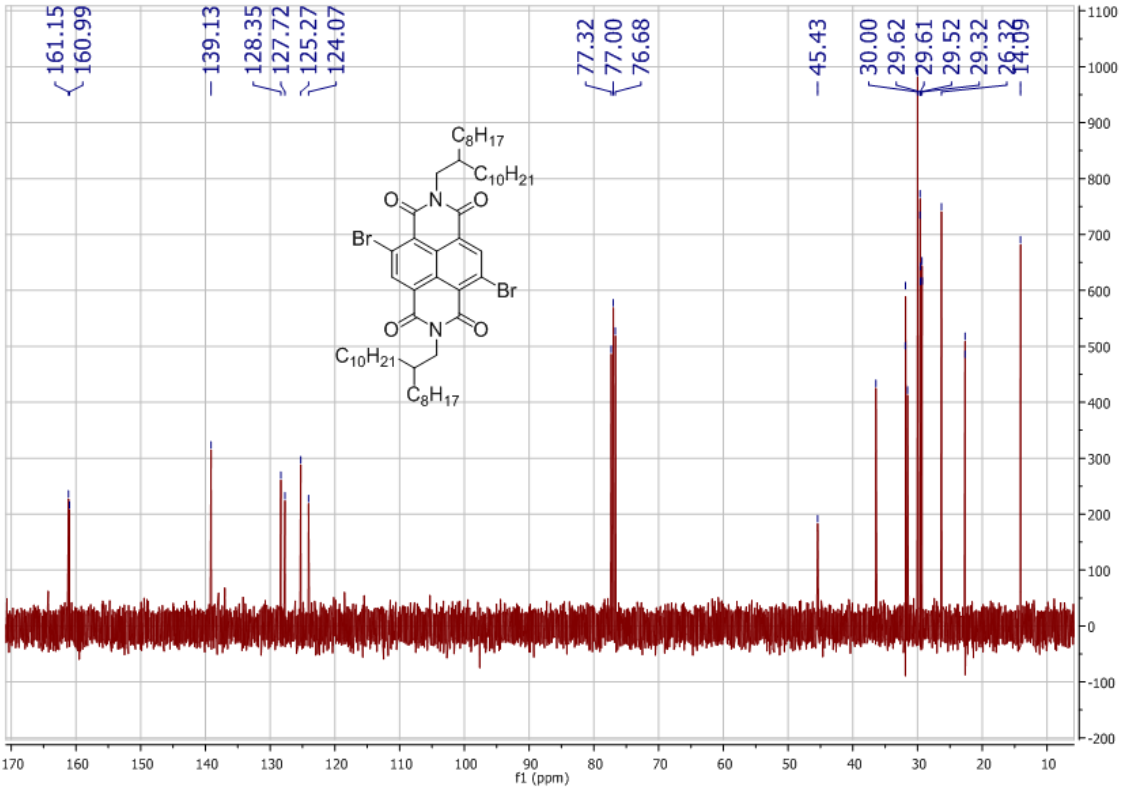

Figure S4. ^{13}C NMR spectrum of compound **(7)** in $CDCl_3$.

2,7-bis(2-octyldodecyl)-4,9-di(thiophen-2-yl)benzo[lmn][3,8]phenanthroline-1,3,6,8(2H,7H)-tetraone (8)

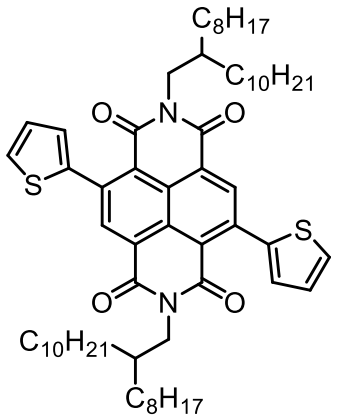

To a stirred solution of 4,9-dibromo-2,7-bis(2-octyldodecyl)benzo[lmn][3,8]phenanthroline-1,3,6,8(2H,7H)-tetraone **(7)** (650 mg, 0.66 mmol, 1.00 eq) in anhydrous and degassed toluene (75 mL), 2-(tributylstannyl)thiophene (490 mg, 419 µL, 1.32 mmol, 2.00 eq) is added under argon. The solution is stirred until reaching complete solubilization prior to the addition of tris(dibenzylideneacetone) dipalladium(0) (31 mg, 33 µmol, 0.05 eq) and tri(o-tolyl)phosphine (20 mg, 66 µmol, 0.10 eq). The reaction mixture is stirred at 110°C overnight and then allowed to cool down to room temperature. The reaction mixture is poured into 1.0 M aqueous HCl and diluted with DCM. The organic layer is washed with 1.0 M aqueous HCl and saturated aqueous NH_4Cl, dried over Na_2SO_4, filtered and concentrated under reduced pressure. The resulting crude product is purified by column chromatography (SiO_2, petroleum ether:DCM - 5:5) affording the pure compound as a deep-red solid (0.56 g, 0.56 mmol, 86 %).

Chemical formula: $C_{62}H_{90}N_2O_4S_2$

Molecular weight: 991.53 g mol^{-1}

^{1}H NMR ($CDCl_3$, 400 MHz, 298 K): δ (ppm) = 8.76 (s, 2H), 7.56 (dd, ^3J = 4.9 Hz, ^4J = 0.8 Hz, 2H), 7.31 (dd, ^3J = 3.5 Hz, ^4J = 0.9 Hz, 2H), 7.20 (dd, ^3J = 5.0 Hz, ^3J = 3.6 Hz, 2H), 4.07 (d, ^3J = 7.3 Hz, 4H), 1.96 (m, 2H), 1.44-1.16 (m, 64H), 0.89-0.84 (m, 12H).

^{13}C NMR ($CDCl_3$, 100 MHz, 298 K): δ (ppm) = 162.5, 162.3, 140.7, 140.2, 136.6, 128.2, 128.0, 127.4, 127.4, 125.4, 123.3, 44.8, 36.4, 31.9, 31.9, 31.5, 31.5, 30.0, 29.6, 29.6, 29.6, 29.5, 29.3, 29.3, 26.3, 22.6, 22.6, 14.1.

All characterization data are in accordance with the literature.[8]

4,9-bis(5-bromothiophen-2-yl)-2,7-bis(2-octyldodecyl)benzo[lmn][3,8]phenanthroline-1,3,6,8(2H,7H)-tetraone (9)

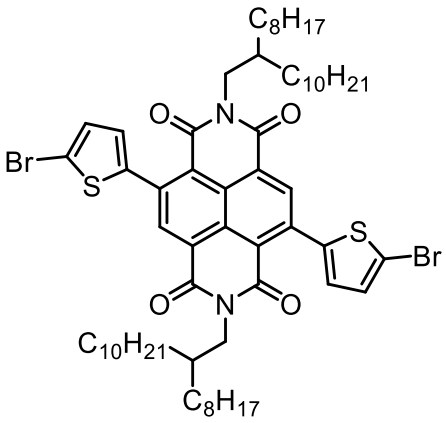

To a stirred solution, of 2,6-bis(2-thienyl)-2,6-naphthalene-1,4,5,8-tetracarboxylic-N,N'-bis(2-octyldodecyl) diimide **(8)** (339 mg, 0.34 mmol, 1.00 eq) in a mixture of glacial AcOH:$CHCl_3$ (1:1 vol%, 50 mL), N-bromosuccinimide (152 mg, 0.85 mmol, 2.50 eq) is added. The reaction mixture is stirred at 60°C for 5h. The reaction mixture is allowed to cool down, concentrated under reduced pressure and diluted with DCM. The organic layer is washed with deionized water, dried over Na_2SO_4, filtered and concentrated under reduced pressure. The resulting crude product is purified by column chromatography (SiO_2, petroleum ether:DCM - 5:5 ; SiO_2, *n*-hexane:diethyl ether - 9:1) affording the pure compound as a deep-red solid (365 mg, 0.32 mmol, 93 %).

Chemical formula: $C_{62}H_{88}Br_2N_2O_4S_2$

Molecular weight: 1149.32 g mol^{-1}

^{1}H NMR ($CDCl_3$, 400 MHz, 298 K): δ (ppm) = 8.72 (s, 2H), 7.14 (d, ^3J = 3.8 Hz, 2H), 7.08 (d, ^3J = 3.8 Hz, 2H), 4.07 (d, ^3J = 7.4 Hz, 4H), 1.94 (m, 2H), 1.44-1.16 (m, 64H), 0.88-0.83 (m, 12H).

^{13}C NMR ($CDCl_3$, 100 MHz, 298 K): δ (ppm) = 162.3, 162.3, 142.2, 139.1, 136.4, 130.2, 128.8, 127.5, 125.6, 123.1, 115.5, 45.0, 36.5, 31.9, 31.9, 31.5, 31.5, 30.0, 29.7, 29.6, 29.6, 29.5, 29.3, 29.3, 26.3, 22.7, 14.1.

All characterization data are in accordance with the literature.[8]

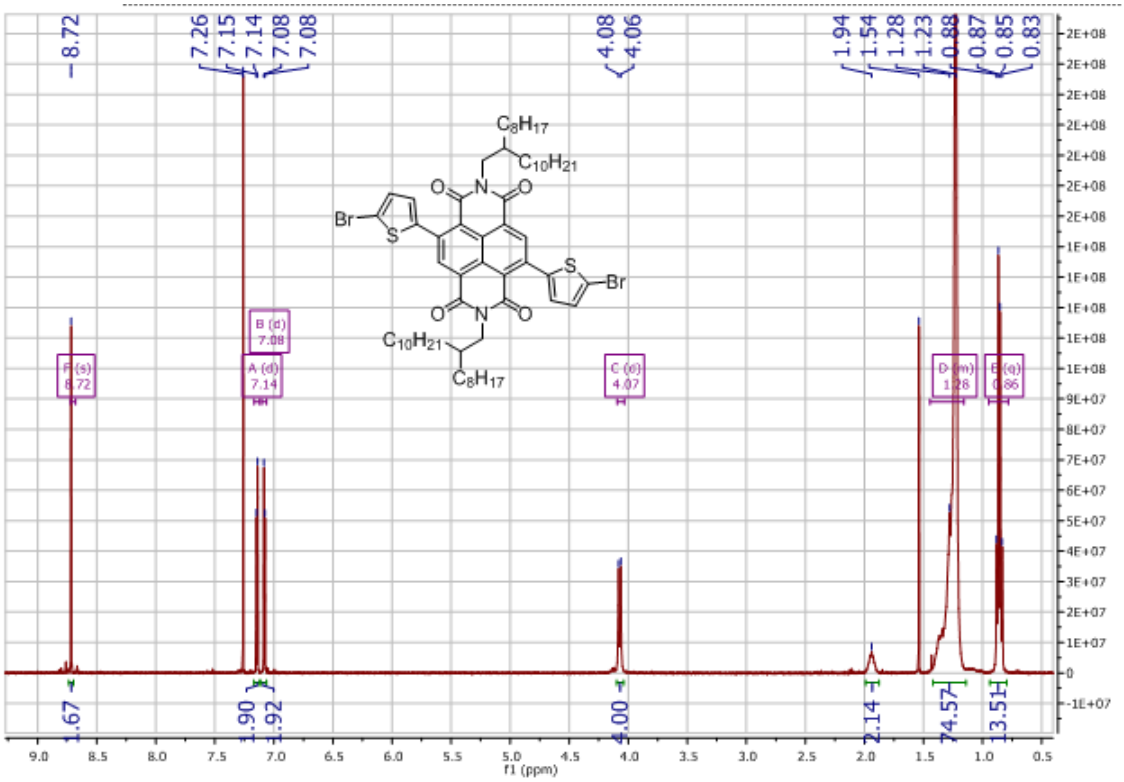

Figure S5. ^{1}H NMR spectrum of compound **(9)** in $CDCl_3$.

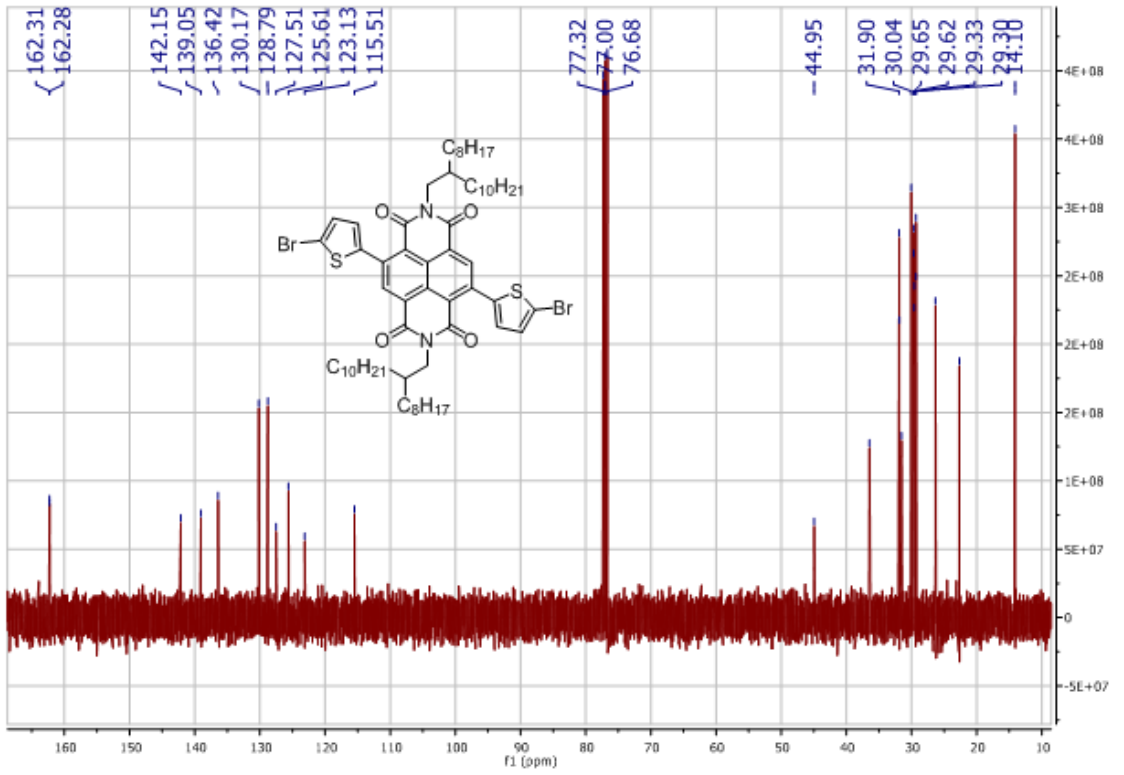

Figure S6. ^{13}C NMR spectrum of compound **(9)** in $CDCl_3$.

1.2. Polymer synthesis

The elemental analysis were carried out respectively on a Flash EA1112 microanalyzer and a Q-Exactive instruments by the CRMPO laboratory (Université de Rennes). See size exclusion chromatography section below for details.

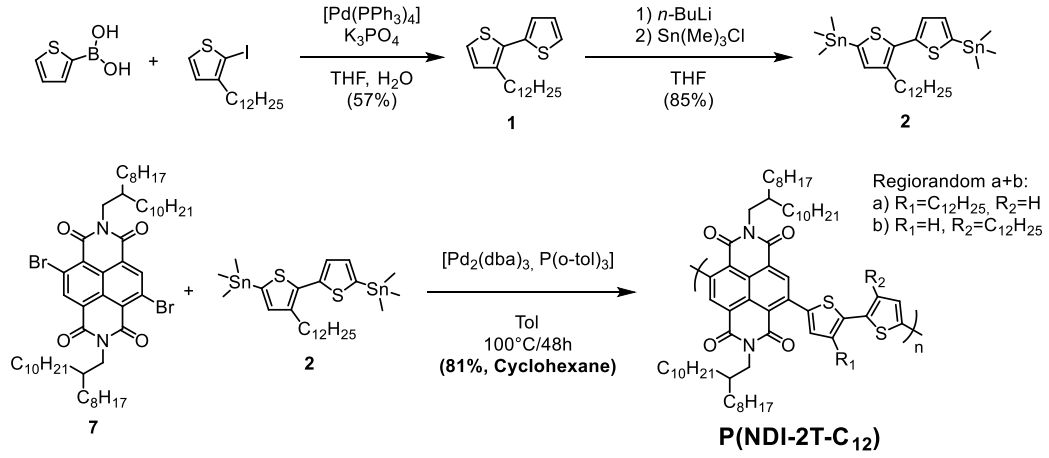

Figure S7. Synthesis route of **P(NDI-2T-C_{12})** copolymer via Stille polymerization.

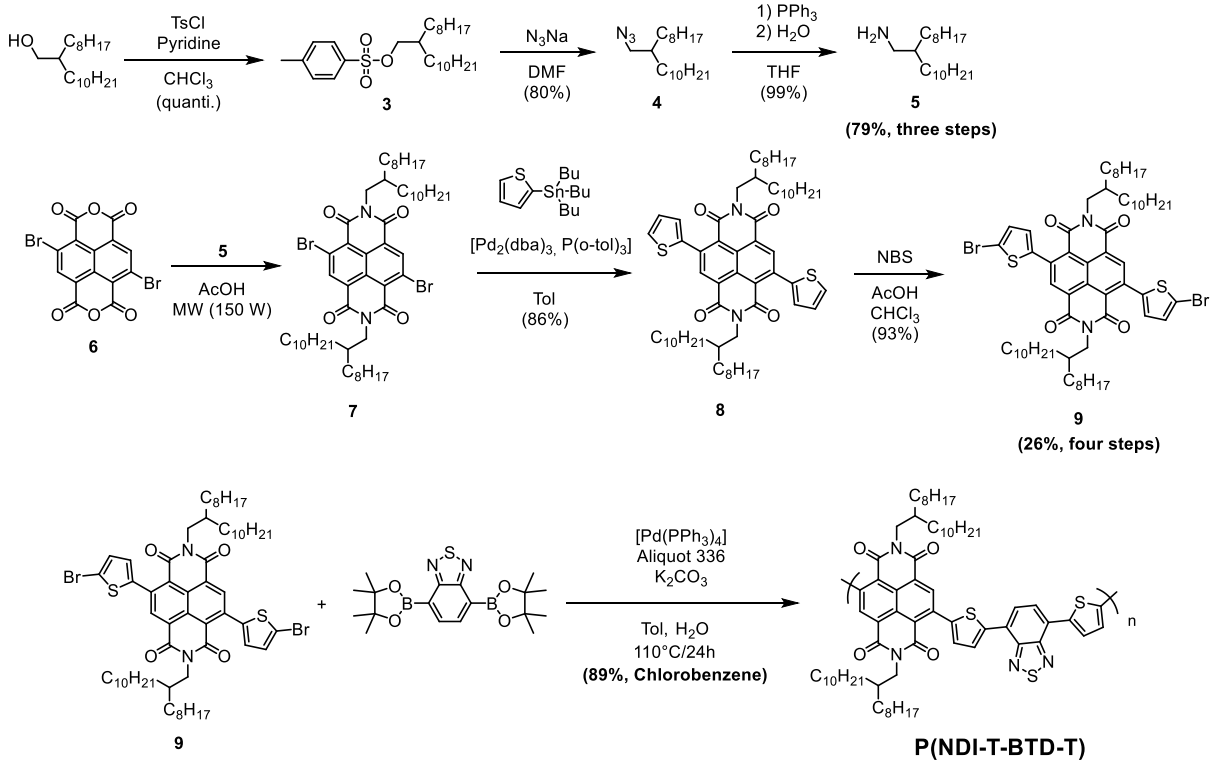

Figure S8. Synthesis route of **P(NDI-T-BTD-T)** copolymer via Suzuki polymerization.

Poly(4-(3-dodecyl-[2,2'-bithiophen]-5-yl)-2,7-bis(2-octyldodecyl)benzo[lmn][3,8]phenanthroline-1,3,6,8(2H,7H)-tetraone) = P(NDI-2T-C_{12})

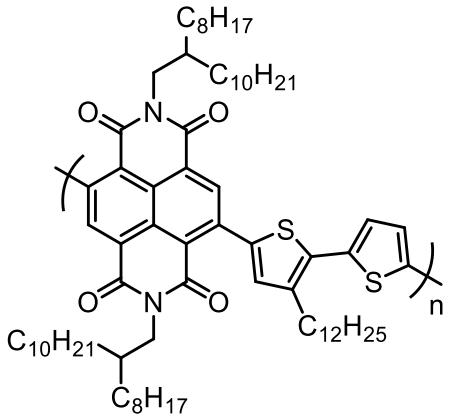

In one Schlenk tube, 4,9-dibromo-2,7-bis(2-octyldodecyl)benzo[lmn][3,8]phenanthroline-1,3,6,8(2H,7H)-tetraone **(7)** (305 mg, 0.31 mmol, 1.00 eq) and (3-dodecyl-[2,2'-bithiophene]-5,5'-diyl)bis(trimethylstannane) **(2)** (209 mg, 0.32 mmol, 1.02 eq) are dried under vacuum 2 h. In a second flask, tris(dibenzylideneacetone) dipalladium(0) (9 mg, 9 µmol, 0.03 eq) and tri(o-tolyl)phosphine (5 mg, 15 µmol, 0.05 eq) are dried under vacuum 2 h. Anhydrous toluene is degassed by freeze-pump-thaw cycling and injected in the Schlenk (22 mL) and in the catalytic system (4x1 mL) under argon. The reactant mixture is degassed by freeze-pump-thaw cycling and stirred prior to the addition of the degassed solution of Pd^0L_2 complex. The mixture is degassed by freeze-pump-thaw cycling a last time, the argon supply is closed to work under pressure and the reaction mixture stirred vigorously at 100°C. After 70 h, end-capping is performed by addition of 2-bromothiophene (60 µL, 0.62 mmol, 2.00 eq). After 20 min at 100°C, tributyl(thiophen-2-yl)stannane (196 µL, 0,62 mmol, 2.00 eq) is added and stirred a further 20 min at 100°C. The reaction mixture is allowed to cool down to room temperature and precipitated dropwise into a 0°C solution of ethylenediamine (103 µL, 1.55 mmol, 5.00 eq) and 15-crown-5 (307 µL, 1.55 mmol, 5.00 eq) in methanol (200 mL) for metal scavenging. The mixture is stirred vigorously overnight at room temperature, filtered through a Soxhlet thimble, washed with methanol (200 mL) and dried under vacuum. Final purification is achieved by Soxhlet extraction successively from acetone, cyclohexane, $CHCl_3$ and toluene. The majority cyclohexane fraction is dried under vacuum, affording the desired polymer as a dark blue solid (291 mg, 0.25 mmol, 81 % with respect to the monomer).

Chemical formula (monomer): $C_{74}H_{114}N_2O_4S_2$

Molecular weight (monomer): 1159.86 g.mol^{-1}

^{1}H NMR ($C_2D_2Cl_4$, 400 MHz, 343 K): δ (ppm) = 8.94-8.64 (aromatic protons), 7.48-7.07 (aromatic protons), 4.31-3.90 (aliphatic protons), 3.18-2.67 (aliphatic protons), 2.13-0.56 (aliphatic protons).

SEC (THF, 313 K, polystyrene calibration): Mn = 8.6 kg mol^{-1}, Mw = 13.6 kg mol^{-1}, Mp = 9.2 kg mol^{-1}, Đ = 1.9.

Elemental analysis: Calcd. for $C_{74}H_{114}N_2O_4S_2$: C, 76.63; H, 9.91; N, 2.42; S, 5.53. **Found:** C, 76.07; H, 9.68; N, 2.27; S, 5.28.

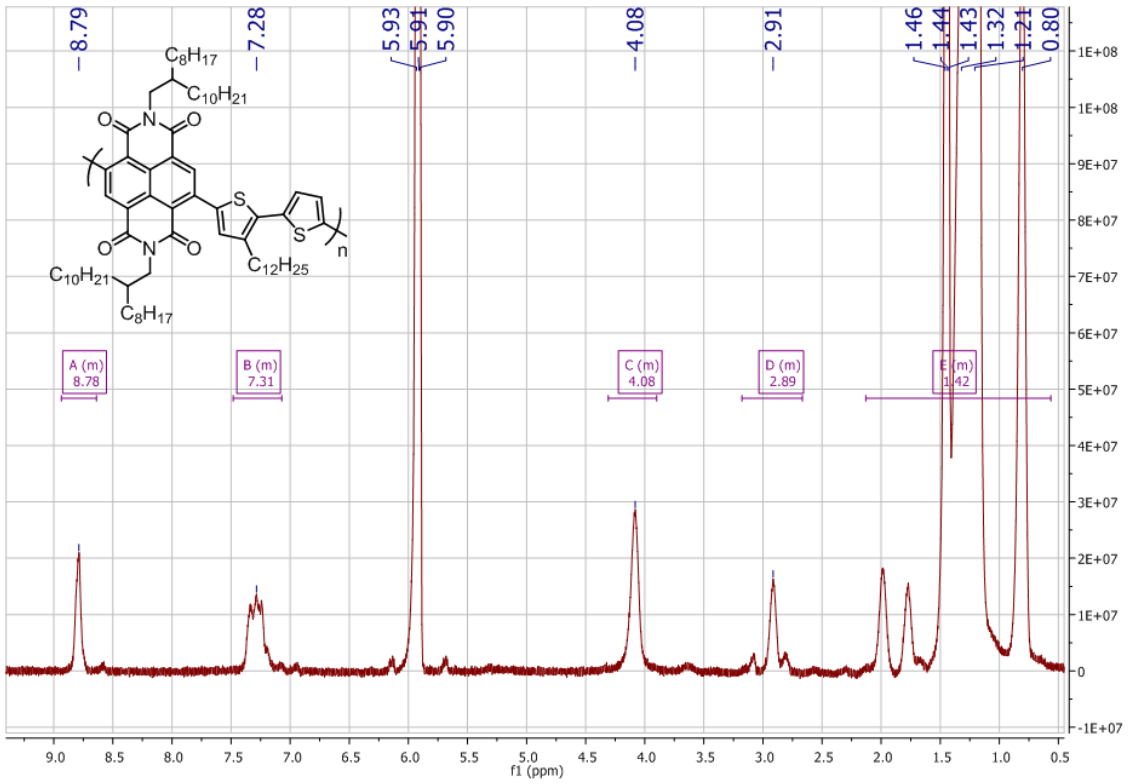

Figure S9. ^{1}H NMR spectrum of **P(NDI-2T-C$_{12}$)** in $C_2D_2Cl_4$.

Poly(2,7-bis(2-octyldodecyl)-4-(5-(7-(thiophen-2-yl)benzo[c][1,2,5]thiadiazol-4-yl)thiophen-2-yl)benzo[lmn][3,8]phenanthroline-1,3,6,8(2H,7H)-tetraone)

= P(NDI-T-BTD-T)

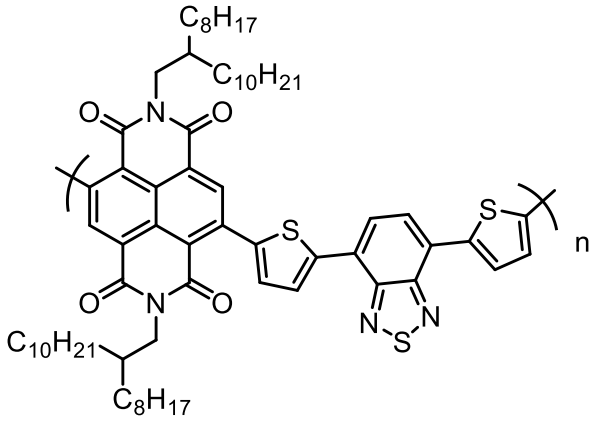

Prior to polymerization, commercially available 2,1,3-benzothiadiazole-4,7-bis(boronic acid pinacol ester) is purified by recrystallization in pentane.

In a Schlenk tube, 4,9-bis(5-bromothiophen-2-yl)-2,7-bis(2-octyldodecyl)benzo[lmn][3,8]phenanthroline-1,3,6,8(2H,7H)-tetraone **(9)** (155 mg, 0.13 mmol, 1.00 eq) and 2,1,3-benzothiadiazole-4,7-bis(boronic acid pinacol ester) (54 mg, 0.14 mmol, 1.04 eq) are dried under vacuum overnight. Then tetrakis(triphenylphosphine)palladium(0) (16 mg, 13 µmol, 0.10 eq), one drop of Aliquat 336, degassed 1.0 M aqueous solution of potassium carbonate (2.7 mL, 2.70 mmol, 20.00 eq) and degassed anhydrous toluene (2.7 mL) by freeze-pump-thaw cycling are added under argon. The mixture is degassed by freeze-pump-thaw cycling, the argon supply is closed to work under pressure and the reaction mixture stirred vigorously at 110°C. After 24 h, end-capping is performed by addition of 2-bromothiophene (26 µL, 0.27 mmol, 2.00 eq) and degassed anhydrous toluene (2 mL). After 4 h at 100°C, 5,5-dimethyl-2-(thiophen-2-yl)-1,3,2-dioxaborinane (53 mg, 0,27 mmol, 2.00 eq) solubilized in degassed anhydrous toluene (2 mL) is added and stirred overnight at 100°C. The reaction mixture is allowed to cool down to room temperature and precipitated dropwise into a 0°C solution of ethylenediamine (45 µL, 0.67 mmol, 5.00 eq) and 15-crown-5 (134 µL, 0.67 mmol, 5.00 eq) in methanol (200 mL) for metal scavenging. The mixture is stirred vigorously overnight at room temperature, filtered through a Soxhlet thimble, washed with methanol (50 mL) and dried under vacuum. Final purification is achieved by Soxhlet extraction successively from acetone, cyclohexane, $CHCl_3$ and chlorobenzene. The majority chlorobenzene fraction is dried under vacuum, affording the desired polymer as a dark blue solid (135 mg, 0.12 mmol, 89 % with respect to the monomer).

Chemical formula (monomer): $C_{68}H_{92}N_4O_4S_3$

Molecular weight (monomer): 1125.69 g mol^{-1}

^{1}H NMR ($C_2D_2Cl_4$, 400 MHz, 343 K): δ (ppm) = 8.97-7.34 (aromatic protons), 4.13 (s, aliphatic protons in alpha of the imide), 2.13-0.58 (aliphatic protons).

SEC (THF, 313 K, polystyrene calibration, filtered 0.45 µm at 313 K): Mn = 64.1 kg mol^{-1}, Mw = 231.5 kg mol^{-1}, Mp = 46.2 kg mol^{-1}, Đ = 4.6.

Elemental analysis: Calcd. for $C_{68}H_{92}N_4O_4S_3$: C, 72.56; H, 8.24; N, 4.98; S, 8.54. Found: C, 78.05 ; H, 11.47; N, 1.91; S, 3.01.

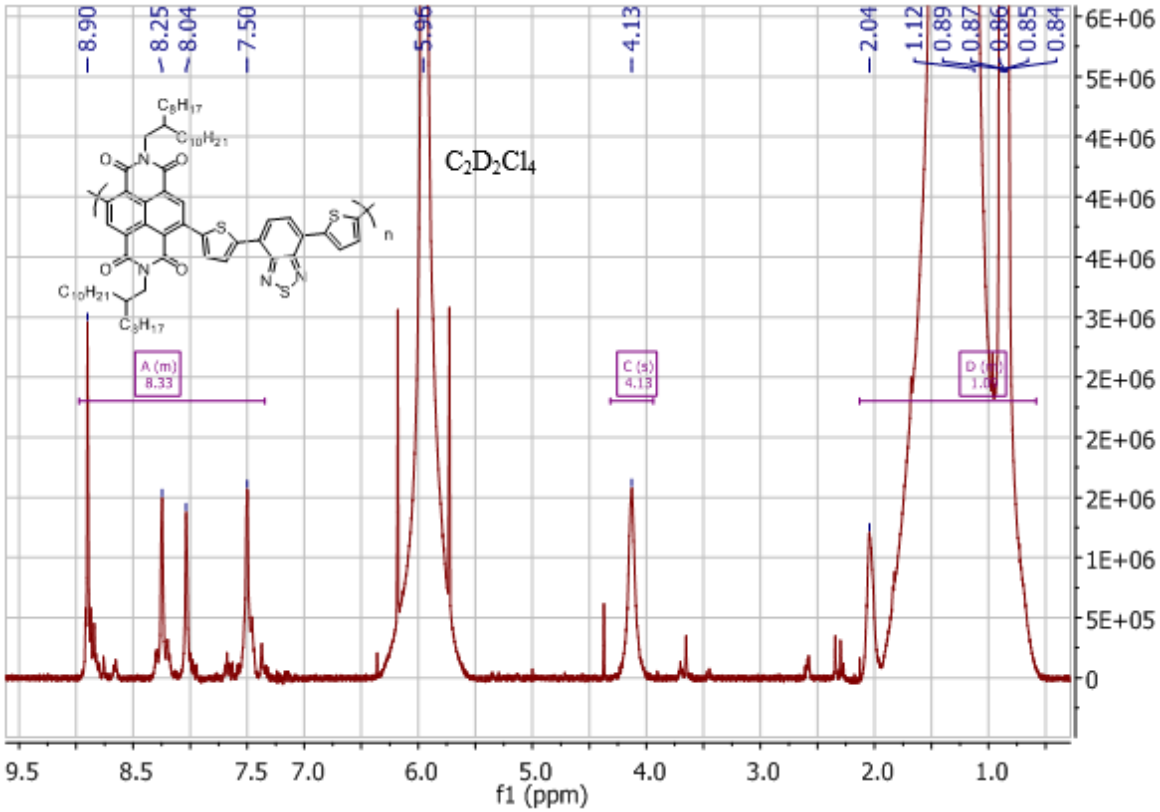

Figure S10. ^{1}H NMR spectrum of **P(NDI-T-BTD-T)** in $C_2D_2Cl_4$.

1.3. Size exclusion chromatography

All the size exclusion chromatography (SEC) experiments were carried out on an Agilent 1260 Infinity II apparatus. The diode array detector was calibrated to the maximum wavelength of absorbance (determined by UV-Vis spectroscopy). THF (99+%, extra-pure, ACROS) at 40°C was used as eluent at 1.0 mL min^{-1}. Insoluble materials were removed by filtration for P(NDI-T-BTD-T) (0.45µm). Mn, Mw and Đ values are extracted using a standard polystyrene calibration (curve fitted with "polynom3", **Figure S11**). The diode array detector was calibrated to the

maximum of absorbance of each compound for a more accurate analysis of each polymer. All the extracted values are summarized in **Table S1** below. The degree of polymerization (DP_n) is calculated according to the definition: ratio of Mn to the molar mass of one repeating unit of the polymer.

Polymer	Fraction	Mn (kg mol^{-1})	Mw (kg mol^{-1})	Mp (kg mol^{-1})	Đ	DPn
P(NDI-2T-C_{12})	Cyclohexane	8.6	13.6	9.2	1.9	8
P(NDI-T-BTD-T)*	Chlotobenzene	64.1	231.5	46.2	4.6	> 57

Table S1. Summary of SEC results (THF, 40°C, *filtered solution 0.45µm).

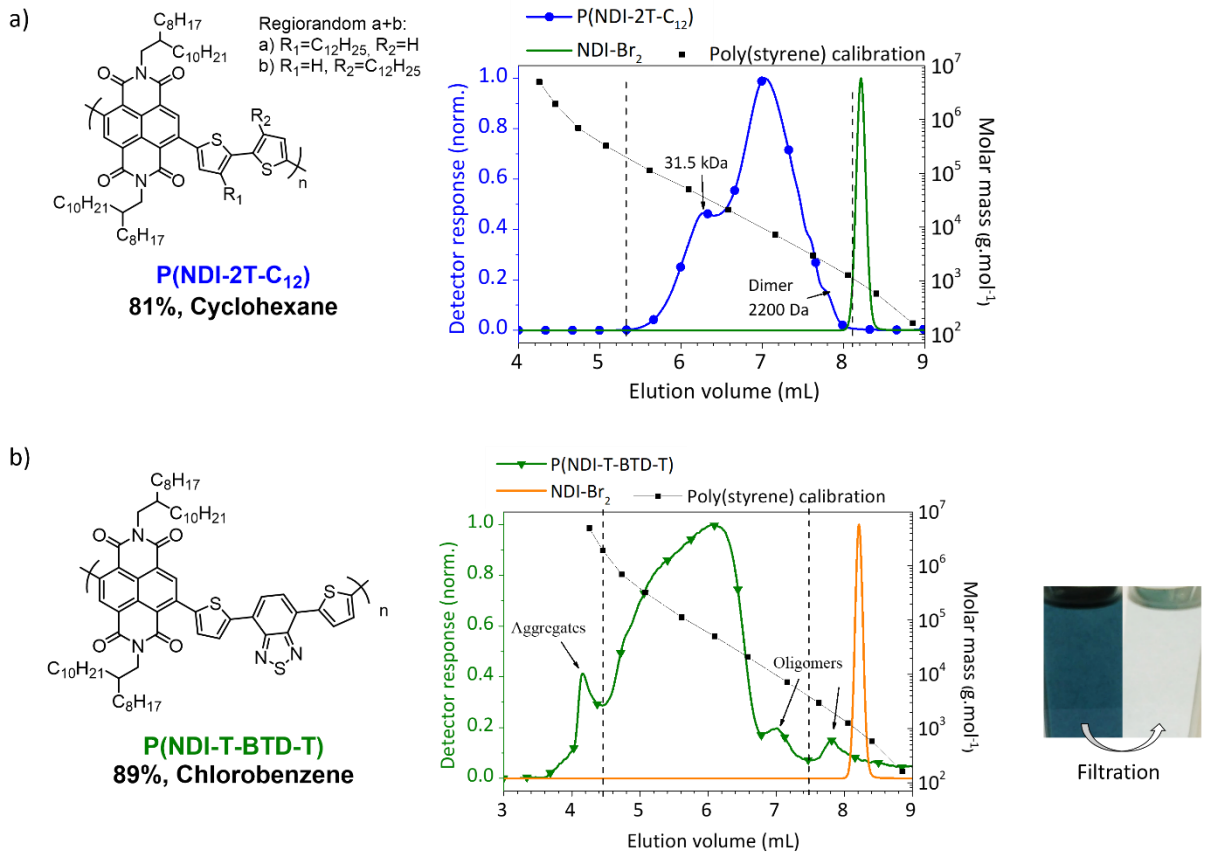

Figure S11. Elugrams (a) of fully soluble **P(NDI-2T-C_{12})** in THF/40°C, and (b) of the filtered solution of **P(NDI-T-BTD-T)** in THF/40°C. Inset: THF solution before and after filtration.

From **Figure S11**a, we see that P(NDI-2T-C_{12}) is mainly composed of a first fraction at 31.5 kg mol^{-1} (~27 units) and a second fraction at 9.2 kg mol^{-1} (~8 units) with a narrow dispersity of Đ = 1.9. In general, for a given material of a given Mn, the smaller the dispersity, the higher the molecular order will be.[9] Hence, low Đ is usually interesting.

In opposition, P(NDI-T-BTD-T) is far less soluble in THF at 40°C. As aggregation is a temperature-controlled process, the solutions were stirred at 40°C and filtered (0.45 µm) before injection. By doing so, we prevented the obstruction of the chromatography column and ensured that the polymer chains analyzed are mainly solubilized, but we also discarded the polymer chains with the higher molecular weights. Consequently, the oligomers detected are overweighed and are not taken into account for the determination of Mn and Đ. In a similar manner, the peak detected around 4 mL – which would correspond to Mn > 10^4 kg mol^{-1} – is attributed to aggregates smaller than 0.45 µm and not considered. On one hand, the higher masses were filtered away which causes underestimation, but on the other hands, the remaining aggregates lead to overestimation of the molecular weight. With this in mind, we tried to report the most accurate values in **Table S1** in the given conditions. Pictures of the solutions before and after filtration are provided to give an idea of the amount of product removed (**Figure S11**b). We see from the pictures that most of the product was not soluble in THF at 40°C and was filtered away. Such low solubility is consistent with the high molecular weight extracted from the SEC measurements (Mn ≈ 64.1 kg mol^{-1}, Mw ≈ 231.5 kg mol^{-1}). The section of the elugram took into account is delimited by vertical dashed lines for visual representation (**Figure S11**b). High degree of polymerization >57 is estimated. The comparison with the synthesis route reported for P(NDI-BTD)[10] tends to confirm the positive impact of reducing the reaction time from 48 hours to 24 hours in the given polymerization conditions. In general, high degree of polymerization is beneficial for high carrier mobility.[11] Such high molecular weights could be measured more accurately using 1,2,4-trichlorobenzene at 140°C.[12]

1.4. Density functional theory

All calculations were performed with the Amsterdam Density Functional (ADF 2017) program. Before synthesizing a molecule, the designed structure was routinely submitted to round-state density functional theory (DFT) calculations to estimate the overall molecular geometry,

the electronic density distribution along the conjugated backbone and the energy levels of the frontier molecular orbitals. As apolar side chains do not contribute significantly phenyl-alkyl and alkyl chains were substituted by phenyl-methyl and by ethyl or propyl chains respectively. The estimated lowest energy conformations determined using Chem3D software were firstly submitted to a more accurate DFT geometry optimization using a combination of Local Density Approximation VWN (Vosko, Wilk, Nusair) and Generalized Gradient Approximation PBE (Perdew-Burke-Ernzerhof) functionals corrected for dispersion using Grimme methodology (Grimme 3) with the TZ2P basis sets (triple zeta + 2 polarization functions) in a continuum polarizable environment modeled through the COSMO model set for acetonitrile. Then, single-point calculations, using the hybrid functional B3LYP (B3: Becke's 3-parameters, $E_{exchange}$ functional + LYP: Lee, Yand, Parr, $E_{correlation}$ functional) with TZ2P sets in acetonitrile solvent phase, were performed on the optimized conformations to extract the HOMO and LUMO energy levels and the electron density distributions. The electron density distribution of the frontier molecular orbitals were generated using ADFview 2016.106.

1.5. Cyclic voltammetry

Cyclic voltammetry (CV) experiments were carried out on a three-electrode setup controlled with EC-Lab V10.44 software. Tetrabutylammonium hexafluorophosphate (NBu_4PF_6, Electrochemical grade, Aldrich), was dried under primary vacuum before addition of the solvent in order to obtain the supporting electrolyte (1×10^{-1} mol.L^{-1}). Reported voltammograms were recorded at a scan rate of 50 or 100 mV s^{-1} without stirring to limit analyte convection. The polymers were drop-casted films on top of the working electrode from chloroform solution for P(NDI-2T-C_{12}) and chlorobenzene for P(NDI-T-BTD-T). A platinum electrode was used as a working electrode (ALS, Tokyo, Japan, diameter 1 mm), which was polished with 0.05 µm alumina on a felt pad, washed with acetone and dried under an argon stream before use. A platinum wire or disk was used as counter electrode. Its specific area was larger than the one of the working electrode to not limit the kinetic reactions occurring at the working electrode. Non-aqueous electrode (Ag/Ag^+) was used as a pseudo-reference electrode. Ferrocene was used as internal reference. The half-wave potential $E_{1/2}(Fc^+/Fc)$ *vs.* $Ag/AgNO_3$ was measured before and after the polymers for accurate internal calibration and ensure no variation of the pseudo-reference electrode during the experiment. Pseudo or non-

reversible redox waves are obtained for both polymers (**Figure 3a** in main text). Thus, the first oxidation/reduction are considered and both signals were acquired separately (different films from the same solution, scan rate 50 mV s^{-1}). The experimental conditions should be carefully controlled for reliable CV measurements.[13] The Nernstian reduction of ferrocenium (Fc^+/Fc) is displayed (black line) and used as internal reference. The signal of the supporting electrolyte (0.1 M [NBu_4][PF_6]) is shown as dotted line, confirming the stability of the acetonitrile for the considered potentials. For the polymers (colored lines), the difference of signal intensity (see insets) varies in function of the film thickness (the thicker giving the more intense signal) and the capacitance of the redox species. In all cases, clear divergences from the capacitive current of the supporting electrolyte are observed. The reduction (E_{red}^{onset}) and oxidation (E_{ox}^{onset}) potentials were extracted using the tangent method. The LUMO level was assimilated to the negative of the electron affinity and the HOMO level to the negative of the ionization potential[14], and calculated as follows:

$$E_{LUMO}\,(eV) \approx -\,E_{EA}\,(eV) = -\,[4.8 + E_{red}^{onset}(V\ vs.\ Fc^+/Fc)] \pm 0.1$$

$$E_{HOMO}\,(eV) \approx -\,E_{IP}\,(eV) = -\,[4.8 + E_{ox}^{onset}(V\ vs.\ Fc^+/Fc)] \pm 0.1$$

All the energy levels are reported in **Table S2**. Note that the uncertainty on these absolute values is considered to be larger than 0.1 eV, but relative comparison can be considered.[14] The oxidation waves exhibit a lack of reversibility for all these materials which is not surprising for n-type materials. Note that both P(NDI-2T-C_{12}) (blue line) and P(NDI-T-BTD-T) (green line) exhibit stepwise one-electron transfers upon reduction.[15] These remarkably stable and reversible reduction waves are assigned to the successive reduction of the NDI moiety (**Figure S12**). The first reduction corresponds to the LUMO level, while the second wave is attributed to the LUMO+1 level. The LUMO+1 of P(NDI-2T-C_{12}) and P(NDI-T-BTD-T) are calculated at *ca.* -3.5 eV and -3.6 eV respectively. Such stability of the anion and di-anion species are valuable for the long-term operation of the targeted devices.

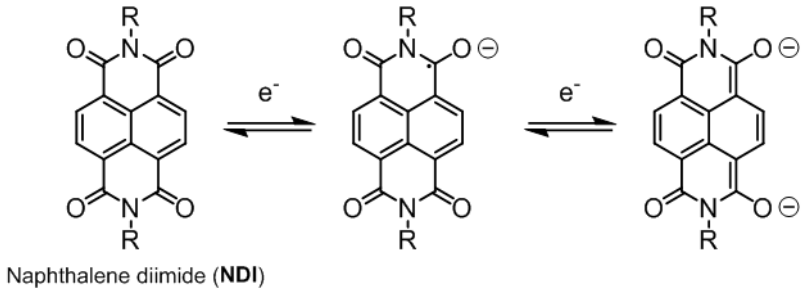

Figure S12. Two-step reduction of the NDI unit. Only one of the resonance structures is represented for clarity.

Polymer	E_{red}^{onset} (V)	E_{ox}^{onset} (V)	E_{LUMO}[a] (eV)	E_{HOMO}[b] (eV)	E_g^{CV}[c] (eV)
P(NDI-2T-C_{12})	- 1.0	+ 1.0	-3.8 (-3.62)	-5.8 (-5.36)	2.0
P(NDI-T-BTD-T)	- 1.0	+ 0.9	-3.8 (-3.63)	-5.7 (-5.39)	1.9

Table S2. Summarize of the values extracted by CV on film. [a,b]Brackets: values calculated by DFT. [a]Calculated by E_{LUMO} (eV) ≈ - E_{EA} (eV) = - [4.8 + E_{red}^{onset}(V vs Fc^+/Fc)]. [b] Calculated by E_{HOMO} (eV) ≈ - E_{IP} (eV) = - [4.8 + E_{ox}^{onset}(V vs Fc^+/Fc)]. [c] Calculated by E_g^{CV} (eV) = $E_{LUMO} - E_{HOMO}$

For comparison purpose, the values calculated by DFT (B3LYP/Grimme3/TZ2P) are reported in brackets in **Table S2** and as dotted lines in **Figure 3b** in main text. We can notice that a systematic overestimation of the calculated LUMOs is of about +0.2 eV. This observation confirms the potential of the DFT for a rational design of n-type copolymers.

1.6. Thermogravimetric analysis

Thermogravimetric analysis (TGA) measures the weight change of a material as a function of temperature in a controlled atmosphere. Measurements were used to evaluate the thermal stability of the polymers up to 500°C. All the experiments were carried out on a SETARAM 92 12 apparatus (SETSOFT software), with a resolution limit of 1 µg. The powders were dried under primary vacuum before loaded (~ 3-5 mg) in a platinum pan. The heating rate was fixed at 10K min^{-1} from RT to 500°C. The atmosphere was controlled by a constant gas flow of N_2 (O2 < 1 ppm). The data are presented in **Figure S13**.

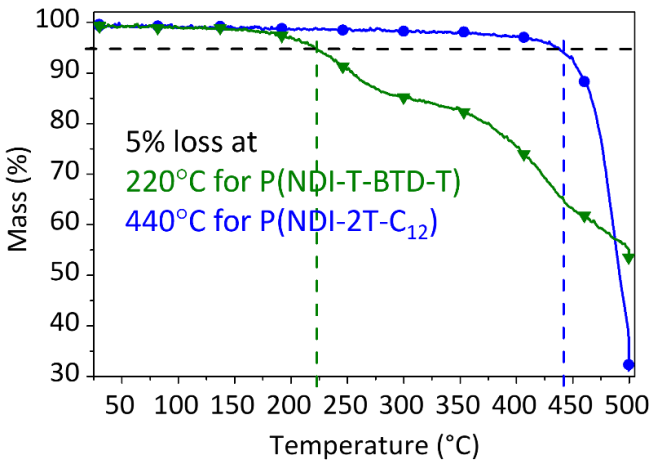

Figure S13. Normalized TGA thermograms acquired at a rate of 10K min^{-1} under N_2 inert atmosphere. Mass corrected with empty pan.

The temperature limit of stability is commonly determinate at 5% loss of mass.[12] The values are reported in insets in **Figure S13**. A flagrant difference between the polymers is observed. P(NDI-2T-C_{12}) (blue line) demonstrates a remarkable stability up to 440°C, thereby confirming its potential use for thermoelectric applications in typical targeted temperature range both organic devices (< 200°C). Conversely, P(NDI-T-BTD-T) (green) thermogram exhibits two inflexions suggesting the sequential degradation of two distinct moieties supposedly due to chain scissions. The first mass losses up to 350°C are tentatively attributed to the partial degradation of the T-BTD-T unit (drawn in red in **Figure S14**). Indeed, the loss is about 20% of the total mass which partly corresponds to the mass percentage of the T-BTD-T moiety compared to the full repeating unit of P(NDI-T-BTD-T). The second onset after 350°C is attributed to the degradation of the rest of the chain. We find that the stability of NDI-based copolymers depends on the comonomer as P(NDI-2T-C_{12}) show remarkable thermal stability, with no apparent degradation up to 350°C. Note that the thermal stability of thin films might be lower due to higher surface-area-to-volume ratio.

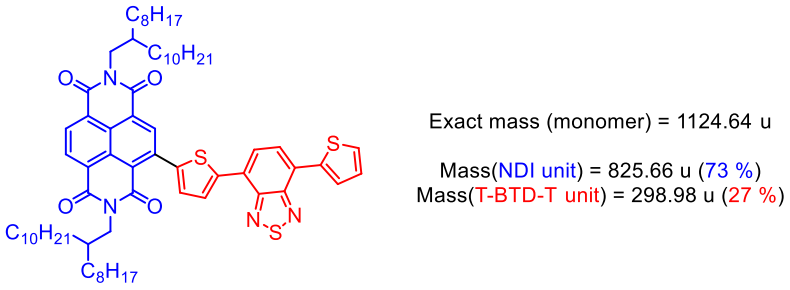

Figure S14. Distribution of the theoretical exact mass in a monomer of P(NDI-T-BTD-T) (n=1, smallest repeating unit).

2. UV-Vis absorbance spectroscopy

The ultra-violet-visible (UV-Vis) measurements were carried out on an Agilent Cary 60 spectrophotometer in ambient conditions.

For solution samples (**Figure 2a** in main text), the polymers were solubilized in chlorobenzene and measured in solution in quartz cuvettes (175−2700 nm) with path lengths of 1 mm. The sample cuvette holder temperature was fixed at 298K using an Agilent Peltier temperature controller.

For solid-state samples (**Figure 2b** in main text), soda-lime glass substrates were sequentially cleaned by sonication in deionized water, acetone, isopropyl alcohol (10min/RT for each step). UV-O_3 treatment was then performed (30 min/RT) to remove hydrocarbon contaminants and to increase the surface tension before spin-coating of polymer solutions using the following spin program:

(step 1) 500 rpm/ 500 rpm s^{-1}/ 10 s

(step 2) 1000 rpm/ 500 rpm s^{-1}/ 80 s

The optical absorption coefficient (α) is calculated using Beer-Lambert relation: $\alpha \approx \frac{2.303\ A}{t}$ (cm^{-1}), with *A* the absorbance and *t* the film thickness assuming that this latter is equivalent to *l* the absorption path length.[16] This equation can be deduced from the definition of the absorbance: $\mathrm{A} = \log_{10}(\frac{I_0}{I})$, with I_0 and *I* the light intensities entering and leaving the absorbing medium respectively.

$I = I_0 e^{-\alpha l} \Rightarrow \frac{I_0}{I} = e^{\alpha l} \Rightarrow \ln\left(\frac{I_0}{I}\right) = \alpha l$, with *l* the absorption path length,

And, $\log_{10}(x) = \frac{\ln(x)}{\ln(10)}$,

$$\Rightarrow \mathrm{A} = \log_{10}(\frac{I_0}{I}) = \frac{\ln\left(\frac{I_0}{I}\right)}{\ln(10)} \approx \frac{\ln\left(\frac{I_0}{I}\right)}{2.303} \approx \frac{\alpha l}{2.303}$$

If $l \approx t \Rightarrow \alpha \approx \frac{2.303\ A}{t}$, with *t* the film thickness.

3. Organic field-effect transistors

The field-effect carrier mobility characterizes the intrinsic ability of a material to conduct charge carriers upon application of an electric field.[17] The evaluation of the in-plane charge carrier mobilities provides valuable information to analyze the conduction properties of a material. We fabricated organic field-effect transistors (OFETs) with neat undoped polymer as semiconducting channel. First, we measured the output characteristics ($f(V_{DS})=I_{DS}$) for different gate voltages (V_{GS}). Then, we defined V_{DS} to operate the transistor in the desired regime (linear or saturation regime) and we acquired transfer characteristics ($f(V_{GS})=I_{DS}$).

Neglecting the dependence of the carrier mobility on V_G and V_D, the carrier mobility in the linear regime can be calculated from:[18]

$$\mu_{lin} = \frac{L}{WC_{ox}V_D}\frac{\partial I_{D,lin}}{\partial V_G}$$

The carrier mobility in saturation regime can be calculated from:

$$\mu_{sat} = \frac{2L}{WC_{ox}}\left(\frac{\partial\sqrt{I_{D,sat}}}{\partial V_G}\right)^2$$

The electron-only OFETs made of P(NDI-2T-C_{12}) and P(NDI-T-BTD-T) were fabricated and measured at ICube in N_2-filled glovebox. Bottom-Gate Bottom-Contact (BGBC) field-effect transistors were elaborated on commercially available pre-patterned test structures whose source and drain contacts were composed of 30 nm thick gold on top of 10 nm thick Indium Tin Oxide (ITO). A 230 nm thick silicon oxide was used as gate dielectric and n-doped (3 x $10^{17}cm^{-3}$) silicon crystal as gate electrode. The channel length and width are 20 or 2.5 µm and 10 mm respectively. Solutions of P(NDI-2T-C_{12}) were prepared in anhydrous toluene at 5.0 mg mL^{-1} and stirred 6 hours at RT. Solutions of P(NDI-T-BTD-T) were prepared in anhydrous chlorobenzene at 5.0 mg mL^{-1} and stirred 6 hours at 100°C. The substrates were cleaned sequentially in an ultrasonic bath using acetone, ethanol and isopropyl alcohol (15 min each step) and subsequently in a ultra-violet ozone system (15 min). Then, hexamethyldisilazane (HMDS) was spin-coated (step1: 500 rpm/200 rpm.s^{-1}/5 s, step 2: 4000 rpm/200 rpm.s^{-1}/50 s) in N_2-filled glovebox and annealed at 130°C/15 min. Finally, the polymer solutions were spin-coated to form the semiconducting channels and complete the device (1500 rpm/200 rpm.s^{-1}/90 s, from RT solutions onto RT substrates except for P(NDI-T-BTD-T): solutions and substrates at 100°C). Back side was cleaned with chlorobenzene. The samples

were then dried overnight under secondary vacuum (<10^{-6} mbar) to remove residual solvent traces. Successive post-deposition annealing of the devices were performed from 80°C to 200°C (stepwise every 40°C, 10 min, in N_2-filled glovebox).

Polymer	Treat-ment	Linear regime			Saturation regime		
		$\mu_{e\ lin}$ ($cm^2\ V^{-1}\ s^{-1}$)	V_{Th} (V)	I_{on}/I_{off}	$\mu_{e\ sat}$ ($cm^2\ V^{-1}\ s^{-1}$)	V_{Th} (V)	I_{on}/I_{off}
P(NDI-2T-C_{12})	as-cast	(5.6 ± 1.4) x 10^{-4}	1	7 x 10^4	(2.1 ± 0.3) x 10^{-3}	0	5 x 10^3
	80°C	(4.3 ± 0.5) x 10^{-4}	1	6 x 10^4	(2.1 ± 0.2) x 10^{-3}	3	1 x 10^3
	120°C	**(5.5 ± 0.9) x 10^{-4}**	**4**	**1 x 10^4**	**(2.2 ± 0.4) x 10^{-3}**	**5**	**3 x 10^2**
	160°C	(2.5 ± 0.02) x 10^{-4}	8	9 x 10^3	(1.1 ± 0.1) x 10^{-3}	13	5 x 10^1
	200°C	(3.2 ± 0.06) x 10^{-4}	9	1 x 10^2	(9.6 ± 0.4) x 10^{-4}	16	1 x 10^1
P(NDI-T-BTD-T)	as-cast*	(6.0 ± 2.3) x 10^{-4}	-2	1 x 10^4	(4.1 ± 2.9) x 10^{-3}	-2	2 x 10^2
	120°C	(8.9 ± 1.3) x 10^{-4}	2	1 x 10^5	(1.6 ± 0.3) x 10^{-2}	3	1 x 10^4
	160°C	(3.0 ± 0.3) x 10^{-3}	2	2 x 10^5	(4.5 ± 1.0) x 10^{-2}	6	2 x 10^4
	200°C	**(4.3 ± 0.3) x 10^{-3}**	**6**	**2 x 10^6**	**(5.3 ± 0.3) x 10^{-2}**	**9**	**3 x 10^4**

Table S3. Summarize of OFET performances obtained for NDI-based polymers. L = 2.5µm, W = 10mm. V_{DS}_lin = +10 V, V_{DS}_sat = +100 V.

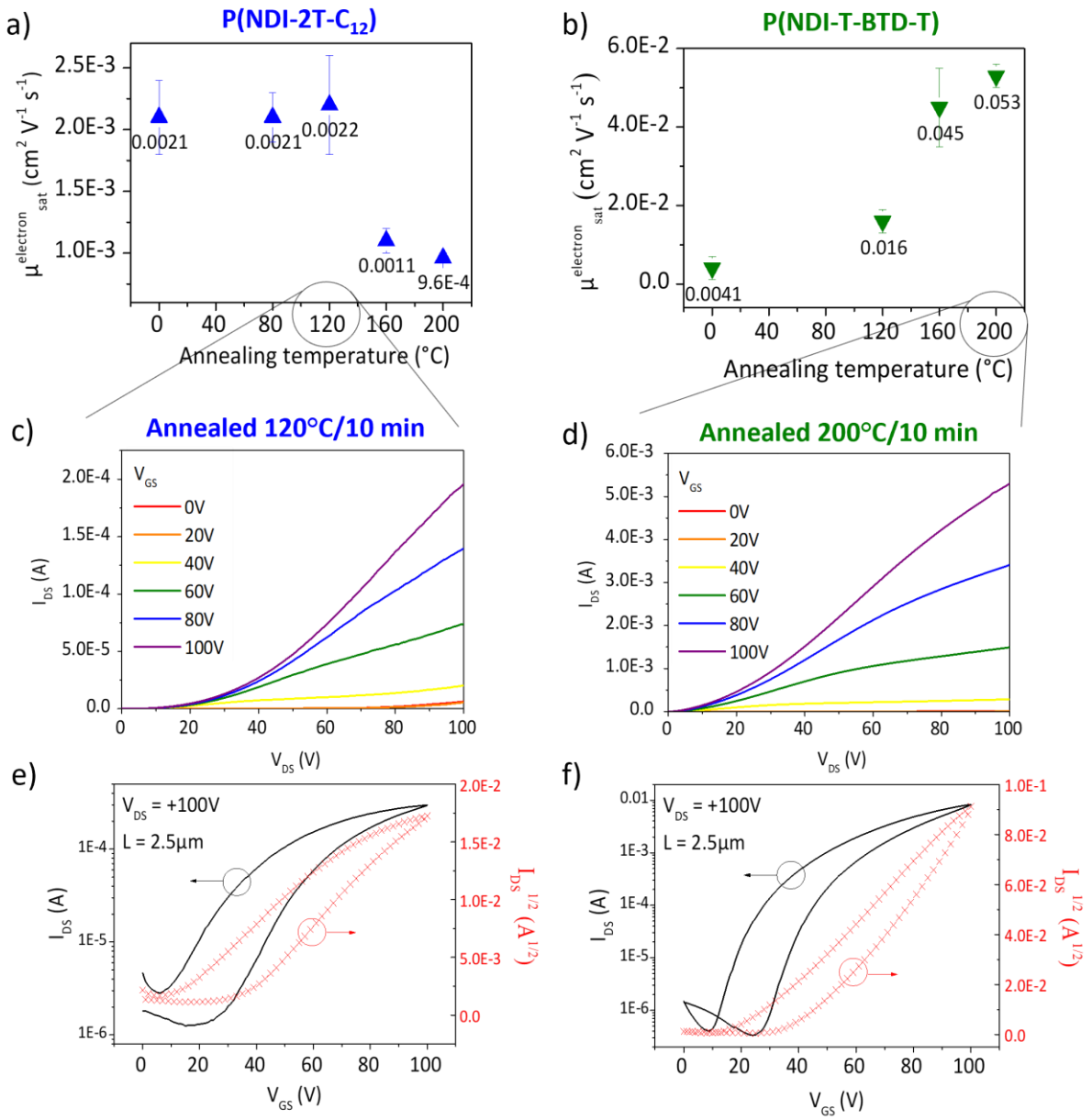

Figure S15. (a-b) Electron mobility in saturation regime (V_{DS} = +100V) as a function of the annealing temperature of P(NDI-2T-C_{12}) and P(NDI-T-BTD-T) BGBC OFETs. (c-d) Output characteristics and (e-f) transfer characteristics for the optimized annealing conditions, being respectively 120°C and 200°C for 10 min.

4. Grazing incidence wide angle x-ray scattering

All neat film preparations were carried out in ambient conditions. P(NDI-2T-C_{12}) was dissolved in anhydrous chloroform at a concentration of 10 mg mL^{-1} and stirred 2 hours at RT before being spin-coated onto a RT clean soda-lime glass substrate (1500 rpm/500 $rpm.s^{-1}$/60 s).

P(NDI-T-BTD-T) was dissolved in anhydrous chlorobenzene at a concentration of 6 mg.mL^{-1} and stirred 2 hours at 110°C before being spin-coated at 110°C onto a 120°C substrate (sample 1 – t ≈ 50 nm: step 1: 600 rpm/300 rpm.s^{-1}/20 s; step 2: 1000 rpm/300 rpm.s^{-1}/80 s – sample 2: 1500 rpm/500 rpm.s^{-1}/60 s). Thermal annealing was performed in inert atmosphere.

The molecular arrangement of these polymers in as-cast and annealed thin films is investigated using grazing incidence wide angle x-ray scattering (GIWAXS). The diffractograms were acquired under ambient atmosphere using a laboratory Rigaku Smartlab diffractometer (Cu rotating anode, $\lambda_{K\alpha}$ = 1.54184 Å). The incident angle was fixed at a small angle (typically ω ≈ 0.2°) to graze the film surface. The interplanar distances were extracting using Bragg's law:

$$\lambda = 2dsin\Theta$$

By performing out-of-plane and in-plane measurements (**Figure S16**), the interplanar distances respectively parallel and perpendicular to the sample surface are determined. For polymers with solubilizing side chains, a diffraction peak at a small angle usually corresponds to lamellar packing distances (20-25 Å). Inversely, a diffraction peak at large angle usually corresponds to close intermolecular stacking (3-4.5 Å) rising from the interaction of neighboring aromatic rings – commonly called π-stacking.[19]

All the GIWAXS diffractograms are presented in **Figure S16** for comparison purpose. All the extracted information are summarized in **Table S4**.

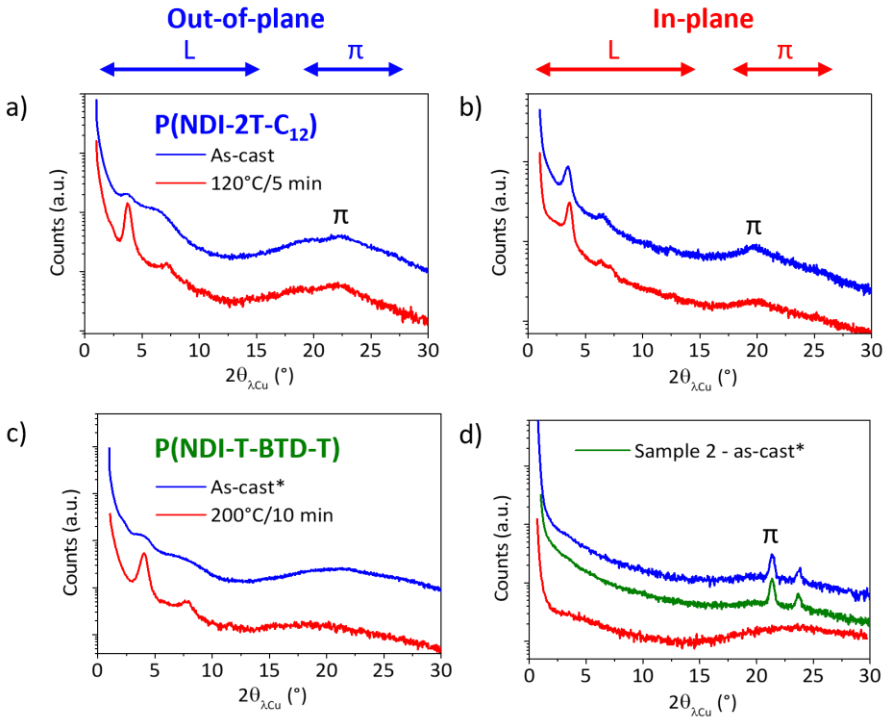

Figure S16. GIWAXS diffractograms of each polymer as-cast and annealed in (a,c) out-of-plane scan and (b,d) in-plane scan of (a-b) P(NDI-2T-C_{12}) and (c-d) P(NDI-T-BTD-T). Conditions of thermal annealing are specified on the graphs.

Polymer	Treatment	Out-of-plane		In-plane		Orientation
		Angle 2Θ (°)	Distance (Å)	Angle 2Θ (°)	Distance (Å)	
P(NDI-2T-C_{12})	as-cast	3.8 (br)	23.3	3.6 (s)	24.5	Lamellar: mixed + **stacking: mixed**
		7.1 (br)	12.5	6.3 (w)	14.0	
		22.2 (br)	4.0	19.8 (br)	4.5	
	120°C/5 min	3.8 (s)	23.3	3.6 (s)	24.5	
		7.1 (w)	12.5	6.3 (w)	14.0	
		22.1 (br)	4.0	7.2 (w)	12.3	
				19.8 (br)	4.5	
P(NDI-T-BTD-T)	as-cast*	4.0 (br)	22.1	21.4 (s)	4.2	Lamellar: edge-on + **π-stacking edge-on?**
		8.0 (br)	11.1	**23.4 (s)**	**3.7**	
	200°C/10 min	4.0 (s)	22.1	-	-	
		8.0 (s)	11.1			

Table S4. Summary of diffraction peaks and corresponding interplanar distances calculated from Bragg's law with $\lambda_{Cu(K\alpha)}$ = 1.54184 Å. The intensity of sharp signals is noted: s = strong, w = weak. Broad signals are always weak, and annotated br = broad. as-cast* = as-cast from hot solutions above 100°C. 'Orientation' corresponds to the most ordered organization obtained

regardless of the annealing treatment. Unsure π-stacking distance is highlighted in **bold**. Broad signals from 15 to 30° include the contribution of the amorphous glass substrate.

According to the peaks found in both out-of-plane and in-plane diffractograms, P(NDI-2T-C_{12}) film exhibits mixed phases. The lamellar interplanar distances (L, **Figure S16** a-b) are similar to the values found in the literature for as-cast N2200[20] (edge-on lamellar packing: 23.3 Å *vs.* 24.9 Å[20], face-on lamellar packing: 24.5 Å *vs.* 24.9 Å[20]). Both out-of-plane and in-plane experiments revealed broad peaks at large angles. By analogy with the broad peak observed for N2200 (3.95 Å[20]), we can assign the peak at ~22.1° (d ≈ 4.0 Å) to face-on π-stacking (π, **Figure S16**a). Note that here the term π-stacking is used to be consistent with the literature but no actual overlap of the π-electron clouds is expected over 3.8 Å.[21] The similarity of 'face-on π-stacking' distances between N2200 and P(NDI-2T-C_{12}) suggests that the introduction of dodecyl chains in position 3 of the thiophene rings preserves the molecular packing properties. Conversely to N2200, a broad peak is observed in in-plane diffractogram of P(NDI-2T-C_{12}) (arrow, **Figure S16**b). This peak indicates periodic planes with an interplanar distance of about 4.5 Å associated to edge-on organization, in accordance with mixed phases.

Compared to P(NDI-2T-C_{12}), remarkably defined peaks at large angles are observed in in-plane diffractrogramms of P(NDI-T-BTD-T) as-cast* thin films (π, **Figure S16**d). Edge-on π-stacking may be enhanced due to the coplanarity of the T-BTD-T unit as shown by DFT (**Figure 3c** in main text). Yet, observing two π-stacking distances is unlikely. If we compare with the literature, we found characteristic distances at 4.2 Å and 3.7 Å (as-cast*) *vs.* 3.82 Å (200°C) associated to edge-on π-stacking. By analogy, we could assign the 3.7 Å distance to enhanced edge-on π-stacking yet OFET results discussed in main text suggest that no π-stacking was achieved. The underlying origins of these peaks is not clear at this stage. It may not originate from polymer-polymer inter-chain interactions. Note that for this poorly soluble polymer, we optimized the deposition conditions by heating up the chlorobenzene solution to 110°C and the substrate to 120°C (as-cast* = as-cast from hot solution). We performed in-plane scans on two different samples deposited from two different solutions. In both cases, the two diffraction peaks at large angles were observed, demonstrating that they are not artefact and that the optimized deposition method is reproducible. One hypothesis can be that chlorobenzene molecules were trapped in an ordered manner in-between the polymer chains

that readily stack when cooling down. Annealing at 200°C caused the loss of the diffraction peaks at large angles but favored the edge-on lamellar packing (22.1 Å (as-cast*) *vs.* 23.1 Å (200°C)[22]) (L, **Figure S16**c). The hypothesis of trapped solvent molecules is surprising considering the relative volatility of chlorobenzene at 110°C, but consistent with the absence of diffraction peak at large angles after annealing the film above the boiling point of chlorobenzene. A clear stacking tendency and advantageous lamellar edge-on orientation were observed, however complementary experiments are required to conclude on the overall packing ability of this material.

5. N-DMBI doping

5.1. Doped sample preparations

All solution and film preparations for doping studies were carried out in nitrogen-filled glovebox (<10 ppm H_2O, O_2) equipped with a molecular sieve solvent trap. Doped samples were prepared by mixing aliquots of freshly prepared host and N-DMBI solutions to reach a constant concentration of host regardless of the dopant concentration. In all cases, N-DMBI solutions were stirred at RT at least 5 minutes in dark inert conditions. Doped solutions were stirred in dark conditions as well. All doped thin films were deposited using the following spin program, similar to undoped films for UV-Vis absorbance spectroscopy:
(step 1) 500 rpm/ 500 rpm s^{-1}/ 10 s
(step 2) 1000 rpm/ 500 rpm s^{-1}/ 80 s

P(NDI-2T-C_{12}) was dissolved in anhydrous toluene at a concentration of 10 mg mL^{-1} and stirred at RT overnight. Specific amount of N-DMBI was added from a toluene solution at 3 mg mL^{-1} or a diluted solution at 1 mg mL^{-1}. Toluene was added to reach host concentration of 5 mg mL^{-1}. The blend solutions were stirred at RT for one hour before being spin-coated at RT onto a RT substrate.

P(NDI-T-BTD-T) was dissolved in anhydrous chlorobenzene at a concentration of 10 mg mL^{-1} and stirred at 80°C overnight to allow complete dissolution. Specific amount of N-DMBI was added from a chlorobenzene solution at 3 mg mL^{-1} or a diluted solution at 1 mg mL^{-1}.

Chlorobenzene was added to reach host concentration of 5 mg mL^{-1}. The blend solutions were stirred at 110°C for one hour before being spin-coated at 100°C onto a pre-heated substrate at 120°C (RT tip).

5.2. Electron paramagnetic resonance

Electron paramagnetic resonance (EPR) spectra were recorded on a Bruker EMX spectrometer (X-band frequency) with an ER-4116 dual mode cavity. The microwave frequency was kept at 9.655 GHz. The parameters of the magnetic fields were chosen to optimize the resolution and the signal-to-noise ratio of the spectra. The magnetic field power and modulation amplitudes are systematically described in the title of the figures.

Solution samples of P(NDI-2T-C_{12}) and P(NDI-T-BTD-T) in toluene and chlorobenzene, respectively, were stirred in N_2-filled glovebox with the optimized amount of N-DMBI to reach the maximum conductivity in thin film. Both solutions have the same total concentration of polymer (5 mg mL^{-1}). EPR samples were prepared by confining aliquots of these solutions in capillary tubes (5 µL total). Samples were taken at RT and after stirring at 120°C/15 min in inert atmosphere. Considering the cavity size of 1.5 cm, the volume of solution sample probed was estimated to be 1.1 µL.

5.3. UV-Vis-NIR absorbance spectroscopy

The UV-Vis-near infrared (NIR) measurements were carried out on a PerkinElmer Lambda 950 spectrophotometer in ambient conditions. The doped film samples were taken from the glovebox to the spectrophotometer in a sealed N_2-filled case, thereby limiting the air exposure to only few minutes during spectrum acquisition.

5.4. Surface morphology: atomic force microscopy

Atomic Force Microscopy (AFM) topography images of N-DMBI-doped P(NDI-2TC_{12}) films were recorded with a Dimension Icon Bruker AFM in peak force tapping mode with ScanAsyst-Air cantilevers (NanoScope software version 9.40) under ambient conditions. The images were treated using WSxM software (version 5.0 Develop 9.1).

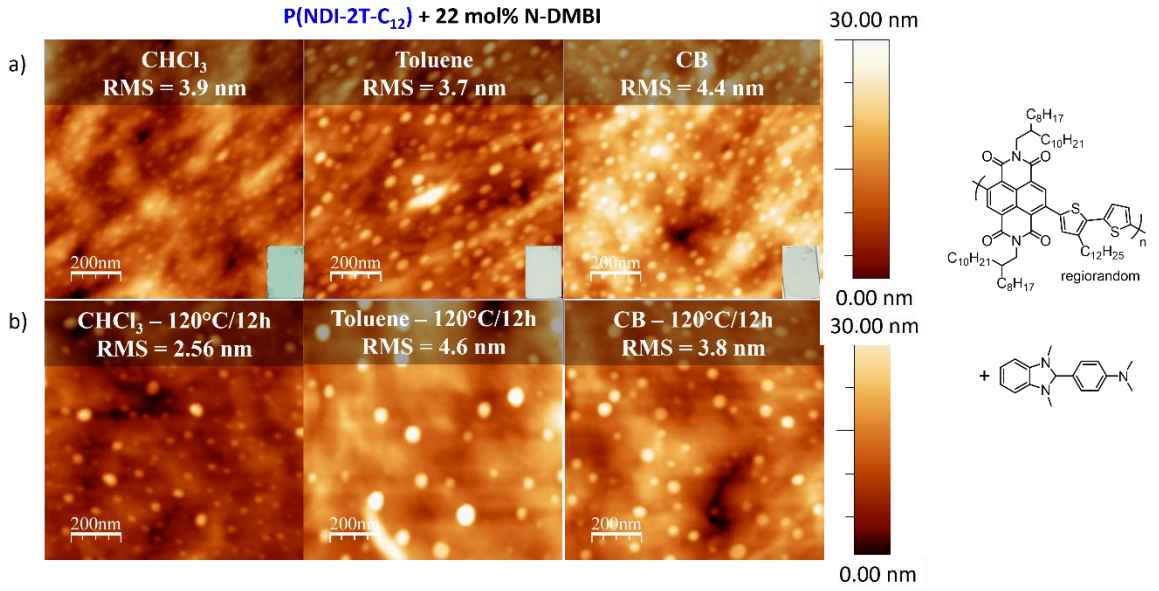

Figure S17. AFM topography images (1.0 x 1.0 µm) of 22 mol% N-DMBI-doped P(NDI-2TC$_{12}$) films (a) before and (b) after annealing.

5.1. Transfer length measurements (TLM)

Transfer Length Measurement is a practical and accurate method for measuring the sheet resistance of relatively resistive layers.[23] Conductivity as low as 10^{-8} S cm^{-1} can be determined on our setup (empirical limit).

Gold-coated (30 nm) poly(ethylenenaphthalate) (PEN) substrates (12 µm) were patterned using photolithography and cleaned in an acetone sonication bath (10 min). Note that no UV-O_3 treatment was performed on PEN substrates. The doped N-DMBI:polymer solution were then spin-coated in N_2-filled glovebox in dark conditions as described above. Post-deposition annealing treatments (1h or 16h/120°C) and I-V measurements were performed in the same glovebox in dark conditions.

One substrate is composed of four channels with a fixed width (W) of *ca.* 14,500 µm and different defined channel length (L) ranging from 150 to 1000 µm (**Figure S18**a). I-V curves were recorded with a Keithley 2400 SourceMeter. The sheet resistance is then extracted from the ohmic region of the I-V curves for each channel. The results are then plotted as a function of the L/W ratio (**Figure S18**b). The intercept of the linear regression line corresponds to twice the contact resistance ($2R_c$) and the slope provides the resistance of the semiconductor itself

(R_{semi}). Knowing the film thickness (t, measured by AFM in tapping mode), we deduce the electrical conductivity: $\sigma = \frac{1}{R_{semi.}.t}$.

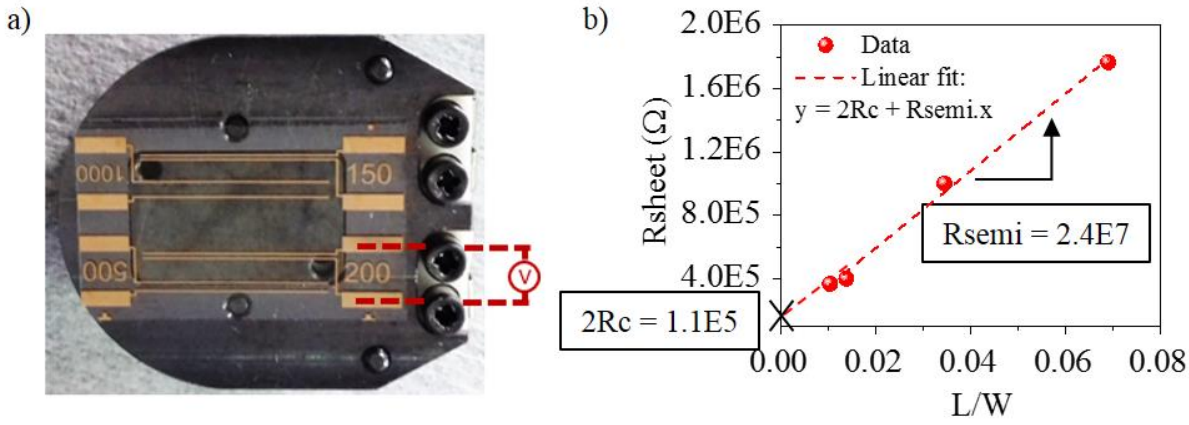

Figure S18. (a) Picture of a TLM substrate with four sets of test contacts for 2-probe measurements. (b) Extraction of the contact resistance and semiconductor resistance.

5.2. Thermoelectric properties of P(NDI-T-BTD-T):N-DMBI (84 mol%)

The polymer-doped samples were deposited by drop casting from chlorobenzene solutions. Thermal activation of N-DMBI was realized *in situ* at 120 °C/16 h before measurements under secondary vacuum. All in-plane thermoelectric parameters (σ, S, κ||) were simultaneously extracted from a single thick film using the Linseis apparatus and the Linseis TA Software (version 2.3.3.36-66-g492333c-d-20190514). The in-plane thermal conductivity was measured using the differential 3ω method. The power factor and ZT were calculated using the following equations:

Power Factor $PF = S^2\sigma$ $ZT = \frac{S^2\sigma}{K} T$

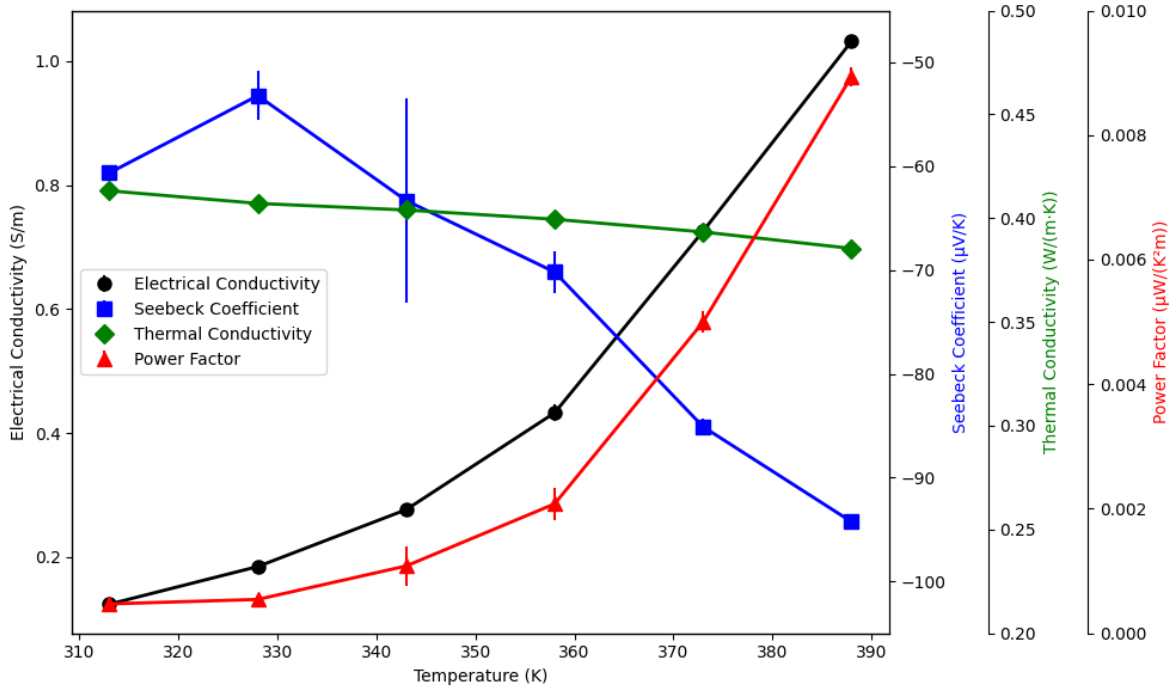

Figure S19. Average thermal and electrical conductivities, Seebeck coefficient, and calculated PF of a P(NDI-T-BTD-T):N-DMBI (84 mol%) doped layer of ≈2.1 ± 0.1 µm within the temperature range of 313–388 K (40-115 °C). Average values over two heating–cooling cycles.

6. Differential Scanning Calorimetry (DSC) analysis

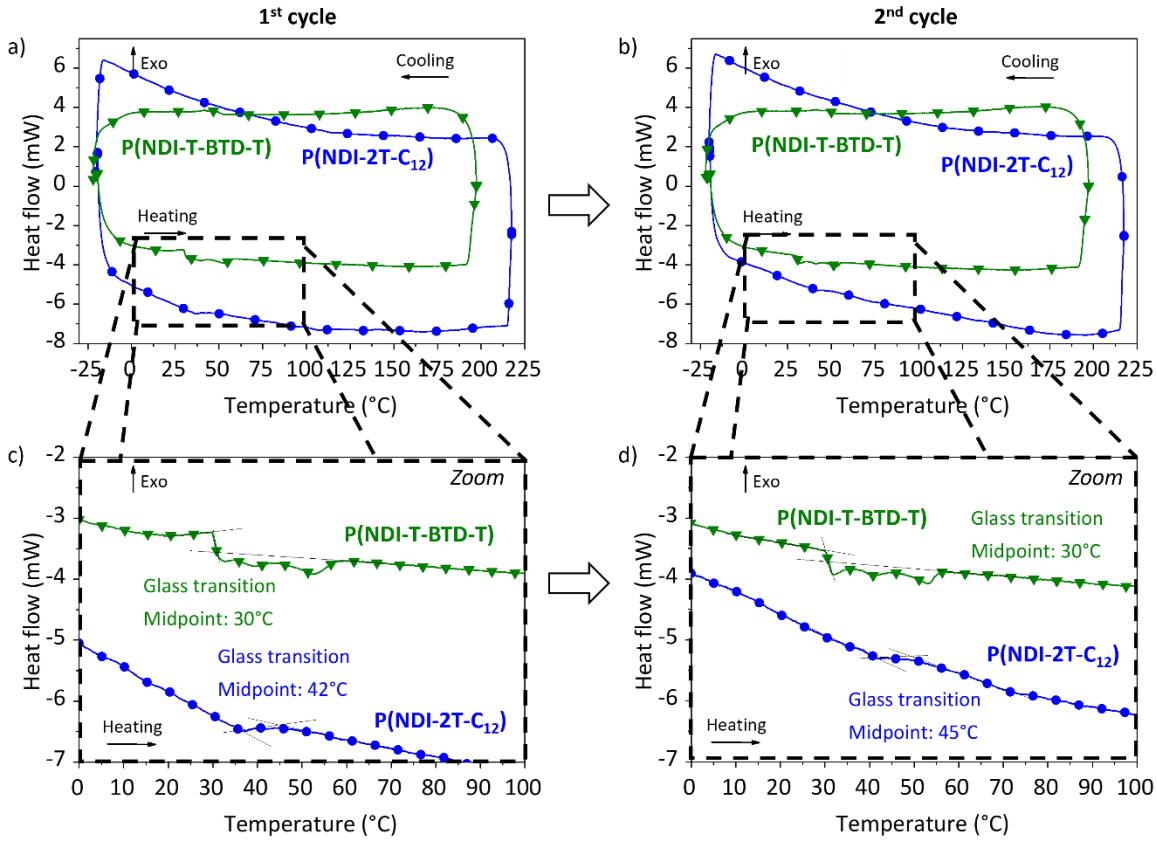

Figure S20. DSC thermograms acquired at a rate of 5 K min^{-1} for P(NDI-2T-C_{12}) and 10 K min^{-1} for P(NDI-T-BTD-T) under N_2 inert atmosphere. Left 1st cycle, right 2nd cycle. (a) Heating and cooling runs, (b) Zoom in the heating run between 0 and 100°C.

For a deeper understanding of the phase transitions that might occur when increasing the temperature, we conducted DSC measurements on pristine dried powders. The experiments were carried out under a constant gas flow of N_2. The first (left) and second (right) cycles are presented in **Figure S20**. For P(NDI-2T-C_{12}) (blue line) we can speculate that the relaxation observed at 45°C corresponds to the glass transition, without certainty. For P(NDI-T-BTD-T) (green line), three consecutive endothermic peaks are observed for both cycles. No precedent was found in the literature. We can tentatively attribute this result to the superposition of melting events and glass transition (~30°C). More advanced DSC technics such as fast scanning (flash) DSC could be performed to confirm (or contradict) the hypothesis made here.

7. References

1 P. Bäuerle, F. Pfau, H. Schlupp, F. Würthner, K.-U. Gaudl, M. B. Caro and P. Fischer, *Journal of the Chemical Society, Perkin Transactions 2*, 1993, 489–494.

2 O. Bardagot, P. Kubik, T. Marszalek, P. Veyre, A. A. Medjahed, M. Sandroni, B. Grévin, S. Pouget, T. Nunes Domschke, A. Carella, S. Gambarelli, W. Pisula and R. Demadrille, *Adv. Funct. Mater.*, 2020, **30**, 2000449.

3 M. C. Hwang, J.-W. Jang, T. K. An, C. E. Park, Y.-H. Kim and S.-K. Kwon, *Macromolecules*, 2012, **45**, 4520–4528.

4 T. Mondal, D. Basak, A. Al Ouahabi, M. Schmutz, P. Mésini and S. Ghosh, *Chem. Commun.*, 2015, **51**, 5040–5043.

5 T. Aytun, L. Barreda, A. Ruiz-Carretero, J. A. Lehrman and S. I. Stupp, *Chemistry of Materials*, 2015, **27**, 1201–1209.

6 C. Thalacker, C. Röger and F. Würthner, *The Journal of Organic Chemistry*, 2006, **71**, 8098–8105.

7 X. Guo and M. D. Watson, *Organic Letters*, 2008, **10**, 5333–5336.

8 C. J. Kudla, D. Dolfen, K. J. Schottler, J.-M. Koenen, D. Breusov, S. Allard and U. Scherf, *Macromolecules*, 2010, **43**, 7864–7867.

9 F. Panzer, H. Bässler, R. Lohwasser, M. Thelakkat and A. Köhler, *J. Phys. Chem. Lett.*, 2014, **5**, 2742–2747.

10 S. Vasimalla, S. P. Senanayak, M. Sharma, K. S. Narayan and P. K. Iyer, *Chemistry of Materials*, 2014, **26**, 4030–4037.

11 R. Noriega, J. Rivnay, K. Vandewal, F. P. V. Koch, N. Stingelin, P. Smith, M. F. Toney and A. Salleo, *Nature Materials*, 2013, **12**, 1038–1044.

12 T. Lei, J.-H. Dou, X.-Y. Cao, J.-Y. Wang and J. Pei, *Adv. Mater.*, 2013, **25**, 6589–6593.

13 N. Elgrishi, K. J. Rountree, B. D. McCarthy, E. S. Rountree, T. T. Eisenhart and J. L. Dempsey, *Journal of Chemical Education*, 2018, **95**, 197–206.

14 C. M. Cardona, W. Li, A. E. Kaifer, D. Stockdale and G. C. Bazan, *Adv. Mater.*, 2011, **23**, 2367–2371.

15 S. K. Lee, Y. Zu, A. Herrmann, Y. Geerts, K. Müllen and A. J. Bard, *Journal of the American Chemical Society*, 1999, **121**, 3513–3520.

16 V. S. Sangawar and N. A. Moharil, *Chemical Science Transactions*, 2012, **1**, 447–455.

17 C. R. Newman, C. D. Frisbie, D. A. da Silva Filho, J.-L. Brédas, P. C. Ewbank and K. R. Mann, *Chem. Mater.*, 2004, **16**, 4436–4451.

18 U. Farok, Y. Falinie, A. Alias, B. Gosh, I. Saad, A. Mukifza and K. Anuar, in *2013 1st International Conference on Artificial Intelligence, Modelling and Simulation*, IEEE, Kota Kinabalu, Malaysia, 2013, pp. 459–461.

19 C. R. Martinez and B. L. Iverson, *Chemical Science*, 2012, **3**, 2191.

20 J. Choi, K.-H. Kim, H. Yu, C. Lee, H. Kang, I. Song, Y. Kim, J. H. Oh and B. J. Kim, *Chemistry of Materials*, 2015, **27**, 5230–5237.

21 C. Janiak, *Journal of the Chemical Society, Dalton Transactions*, 2000, **0**, 3885–3896.

22 C. Gu, W. Hu, J. Yao and H. Fu, *Chemistry of Materials*, 2013, **25**, 2178–2183.

23 L. Giraudet, S. Fauveaux, O. Simonetti, C. Petit, K. Blary, T. Maurel and A. Belkhir, *Synthetic Metals*, 2006, **156**, 838–842.